Available online at www.sciencedirect.com
ScienceDirect
Coordination Chemistry Reviews 252 (2008) 2292–2313
COORDINATION CHEMISTRY REVIEWS
www.elsevier.com/locate/ccr

Review

Solution structure, dynamics and speciation of perfluoroaryl boranes through ^{1}H, ^{11}B and ^{19}F NMR spectroscopy

Tiziana Beringhelli *, Daniela Donghi, Daniela Maggioni, Giuseppe D'Alfonso

Dipartimento di Chimica Inorganica, Metallorganica e Analitica Università degli Studi di Milano, Via Venezian 21, 20133 Milano, Italy

Received 16 November 2007; accepted 15 January 2008
Available online 26 January 2008

Contents

Abstract

Multinuclear NMR spectroscopy has been used to study the solution properties of several perfluoroaryl borane derivatives. The information obtained from all the NMR active isotopes present in these molecules made it possible to establish not only chemical identity, structure and dynamics of their reaction products, but also the complexity of the solution speciation. In other words, multinuclear NMR helped in unravelling the real forms in which they are present in solution, that in some cases can change dramatically according to even slight changes of the solution conditions. Examples will be presented related to the chemistry of tris(pentafluorophenyl)borane, $B(C_6F_5)_3$, and bis(pentafluorophenyl)borinic acid, $B(C_6F_5)_2OH$.

Keywords: Perfluoroaryl boranes; NMR spectroscopy; Lewis acids; Hydrogen bonds; Dynamical behaviour

* Corresponding author. Tel.: +39 02 50314350; fax: +39 02 5031 4405.
E-mail address: tiziana.beringhelli@unimi.it (T. Beringhelli).

0010-8545/$ – see front matter © 2008 Elsevier B.V. All rights reserved.
doi:10.1016/j.ccr.2008.01.018

1. Introduction

Organo-boron derivatives have become increasingly important for their widespread chemical applications [1–5]. In particular, the Lewis acidity of fluoroaryl boranes has been widely exploited in organic synthesis and catalysis [6]. Much of the work focused on tris(pentafluorophenyl)borane BAr_3 (**1**, $Ar = C_6F_5$) [7], but also related molecules such as bis(pentafluorophenyl)borinic acid Ar_2BOH (**2**) [8] have been extensively investigated.

X-ray structures of many derivatives have been obtained, but NMR spectroscopy proved to be a fundamental tool to understand and clarify what was really going on in solution, disclosing the different features of each system studied. We report here some observations (sometimes quite unexpected) concerning the solution behaviour of the two boranes **1** and **2**, coming essentially from our multinuclear NMR studies.

2. The strong Lewis acidity of tris(pentafluorophenyl)borane

Tris(pentafluorophenyl)borane [7] (**1**) is a strong Lewis acid, its strength being comparable to the one of BF_3 [9–11]. Its use as a catalyst or a stoichiometric reagent for organic and organometallic transformation is now well established [6,11–13] but it was primarily employed as a co-catalyst in metallocene-mediated olefin polymerization for its ability to abstract an alkyl group from the metallocene precursor and stabilize, through an ion pair interaction, the active cationic species formed accordingly [14,15]. The details of the polymerization process depend on the complex interplay between the nature of the ligands on the precursor metal complex, its symmetry, the stability and the dynamics of the ion pair formed after the activation [10,16]. Therefore during these last years many reports have appeared in the literature concerning the properties of the adducts generated from the interaction of BAr_3 with different metallocenes and/or with bases [10–16].

Our studies contributed to this multifaceted subject through the characterization of the structure and dynamics (i) of the ion pairs formed by the interaction of BAr_3 with indenyl dimethyl zirconocenes, (ii) of new co-catalysts obtained by reacting BAr_3 with *N*-heterocycles and (iii) of the adducts with water, a possible contaminant in the reaction mixtures in which BAr_3 is applied.

2.1. The interaction of $B(C_6F_5)_3$ with bisindenyl zirconocenes

2.1.1. The preferred rotamers of two highly mobile π ligands

The two ion pairs $[L_2ZrMe]^+[MeBAr_3]^-$ (**3a** L = 4,7-Me_2indenyl, **3b** L = indenyl, Chart 1), are readily formed upon addition of 1 equiv of BAr_3 to toluene solutions of the precursor metallocene complexes. They exhibit apparent C_s symmetry even in the lowest temperature ^{1}H NMR spectra, indicating that, in these complexes, the unsaturated rings enjoy significant conformational freedom [17]. Proton 2D NOESY spectra at ca. 200 K, however, showed that the rotation around the Zr-indenyl

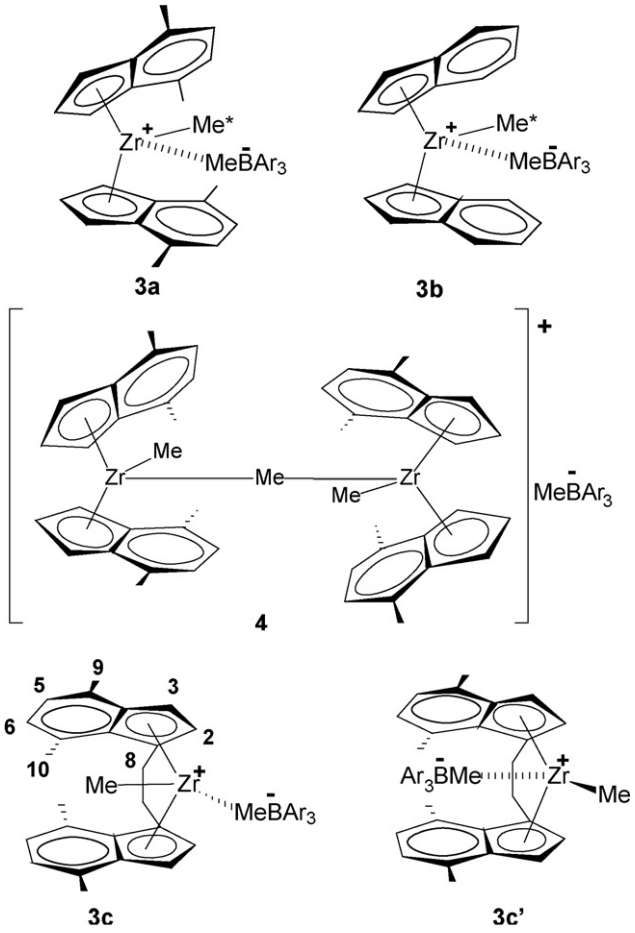

Chart 1.

axis was not completely free, since specific and not generalized dipolar correlations were observed between the indenylic protons and the Me–Zr and Me–B groups (Fig. 1).

This suggests that the two ligands likely swing between limiting conformations. We also observed some NOE cross peaks that can arise only from *inter*-ring contacts (see for instance Me_8/H_2 in Fig. 1). In principle, these NOEs could set constraints on the

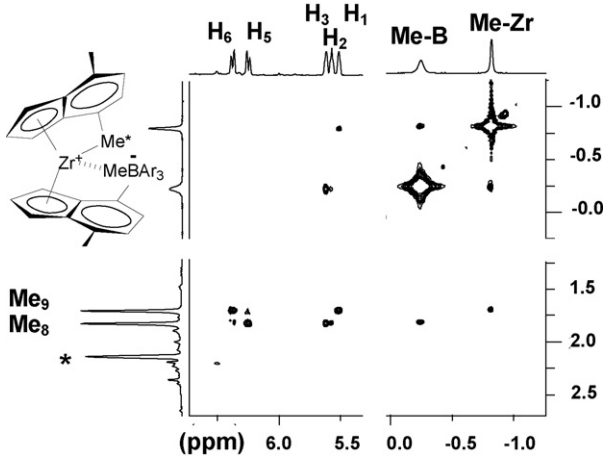

Fig. 1. Selected regions of a ^{1}H NOESY experiment on compound **3a** (211 K, toluene-d_8). The asterisk indicates a solvent resonance. Figure reproduced from ref. [17], with permission of the copyright holders.

relative conformation of the two ligands [18], but the possible presence of different fast exchanging rotamers did not allow to directly convert this information into proton/proton distances.

Insights into the limiting conformations of the two complexes could be obtained using the experimental NOE findings as reference for a molecular mechanics study. Assuming the usual chiral conformation for the BAr_3 fragment, two torsional angles are enough to describe completely the structure of these complexes. On varying stepwise these angles, different structures were obtained and their geometry was optimized using a force field parameterized on purpose of describing these type of ions [17]. For each structure, effective proton/proton distances have been computed, taking into account the averaging due to the dynamic processes, and the expected relative NOEs were compared with the experimental ones. As a result, for both the ion pairs two torsional isomers were found enough to account for all the experimental NOEs. The structures found for **3b** are shown in Fig. 2.

Therefore, even if the rapid motion of the π ligands cannot be frozen on the NMR time scale, the combination of molecular mechanics, using a properly parameterized force field, and experimental NMR data provided clues on the solution conformations of the ion pairs.

2.1.2. Intermolecular contributions to ion pair symmetrization

In these complexes the cation/anion interaction is relatively tight, as proved by the dipolar correlations commented above. However, on rising the temperature, two dynamic processes become evident in the 2D EXSY and 1D spectra.

The first one, above 250 K, exchanges all the diastereotopic ^1H and ^{13}C resonances of the indenylic moieties. The second, detectable only above 300 K, exchanges the Me–B and Me–Zr resonances too. Similar processes have been described for other metallocene complexes [15,19–21] and involve the borane moiety through (i) $[MeBAr_3]^-$ dissociation from the ion pair and its recombination after Me–Zr flip (ion pair separation process, *ips*), leading to the equalization of the diastereotopic resonances on the π ligands *only* and (ii) neutral BAr_3 migration between the two methyl groups (dissociation–recombination process, *d–r*), which interchanges *also* the two Me resonances [19] (Scheme 1).

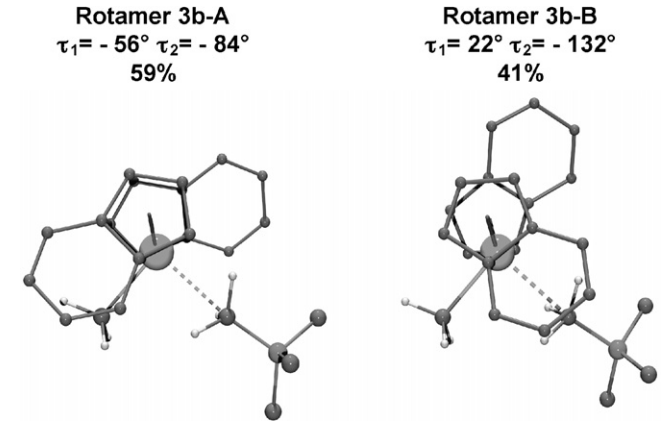

Fig. 2. Top views of the proposed structures for the preferred rotamers of the ion pair **3b**. The values of the torsional angles defining the structures and the relative abundance of each rotamer are reported. Figure redrawn from ref. [17], with permission of the copyright holders.

Rate constants for these two processes were obtained by dynamic band shape analysis [22] and/or by 2D EXSY spectra [23,24] and the *ips* process resulted faster (ca. three orders of magnitude) than *d–r*, as observed also for the ion pairs formed by BAr_3 with other zirconocenes [19].

However, when the ion pairs are prepared directly in the NMR tube, intermolecular $[MeBAr_3]^-$ and BAr_3 exchange processes can give rise to spectroscopic modifications similar to those described above for the two intramolecular processes.

In particular, the presence of even minimal amounts (practically undetectable in ^1H 1D spectra) of cationic impurities, which form loose ion pairs with $[MeBAr_3]^-$, increased the rate of indenyl symmetrization (pseudo *ips* process). The presence of an intermolecular contribution to this exchange was revealed by the concentration dependence of the rate constants and of the bandwidth of the Me–B signal (while that of the Me–Zr signal remained constant). The latter effect implies the existence of an exchange partner for the $[MeBAr_3]^-$ fragment. Indeed, even if not visible in 1D spectra, a $[MeBAr_3]^-$ anion (at δ typical for $[MeBAr_3]^-$ in loosely bound ion pairs [25]) can be indirectly detected in 2D EXSY spectra through its small, broad but unambiguous cross peak with the (tightly bound) $[MeBAr_3]^-$ of **3**. Dilution experiments proved, and allowed us to quantify, the intermolecular contribution to the anion exchange rate. Intermolecular exchange involving the $[MeBAr_3]^-$ anion was much more evident [17] in samples obtained by using less than one equivalent of BAr_3, in which dinuclear methyl bridged cations [26–28] with a loosely bound $[MeBAr_3]^-$ anion, are present (**4** in Chart 1).

When the ion pairs are isolated and purified the observed exchange processes are truly intramolecular. Instead when the products of the reaction are prepared and studied directly in the NMR tube, small impurities can give rise to spurious effects. This difference might account for the conflicting evidence concerning these dynamic processes that has appeared in the literature [10,21].

No concentration dependence of the borane exchange rate (process *d–r*) was found for the samples generated *in situ*. However, differently from that reported for other metallocenes [10], an excess of BAr_3 increased the *d–r* rate. This suggests a bimolecular mechanism, with the possible formation (at least in the transition state) of a dicationic species, likely stabilized by the high donor power of the indenyl ligands.

2.1.3. The attack of $B(C_6F_5)_3$ on a buried methyl group

In *meso ansa*-(bisindenyl)zirconocene, the presence of the bridge locks the indenyl groups in an "eclipsed" conformation and makes the alkyl substituents on the metal atom unequivalent: one (called "outward") points away from the π ligands pocket, while the other one ("inward") lies within the π ligand pocket. The reaction with BAr_3 in principle could give rise to two isomers, according to which alkyl group has been abstracted. The "inward" site is expected to be effectively screened from the attack of the bulky borane, and theoretical calculations on

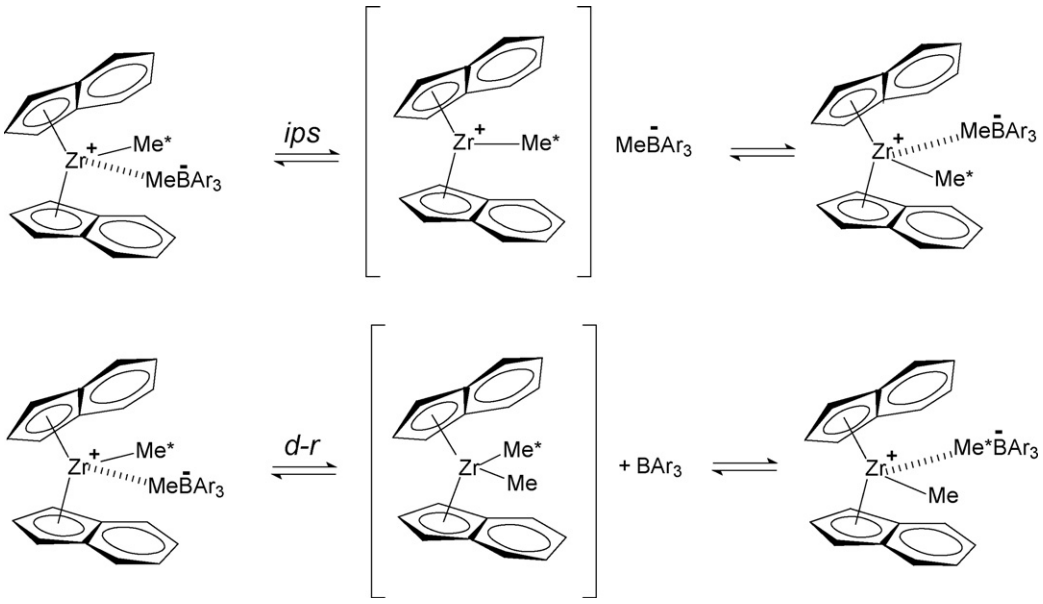

Scheme 1.

similar compounds supported this view [29]. Indeed the contact ion pair *meso*-$[C_2H_4(4,7\text{-}Me_2Ind)_2ZrMe_{inw}]^+[MeBAr_3]^-$ (**3c** in Chart 1) is formed upon reaction of BAr_3 with the corresponding metallocene [30]. The attack of BAr_3 to the more accessible "outward" position is proven by several observations, among which is the sharp signal of the residual "inward" Me–Zr group lying at high-field (δ −1.82) due to the shielding of the ligand π electrons.

However, a careful analysis of ^{1}H NOESY/EXSY at 320 K also revealed the existence of the *meso*-$[C_2H_4(4,7\text{-}Me_2Ind)_2ZrMe_{out}]^+[MeBAr_3]^-$ isomer (**3c′**), as an 'almost hidden' exchange partner of the major species (Fig. 3). The amount of this isomer was ca. 4% and its indenyl resonances were identified through their exchange cross peaks with the corresponding signals of the major isomer. Diagnostically, in **3c′** the broad Me–B resonance is at δ −1.6 and the NOE correlations of its methyl groups are reversed with respect to the major species **3c**.

Both the dynamic processes discussed above for the non *ansa* metallocenes are able to interconvert the two isomers, but the exchange pattern of the methyl groups can clearly discriminate between the two. Indeed the *ips* mechanism would bring the "outward" Me–B in the "inward" position giving rise to $(Me–B)_0 \leftrightarrow (Me–B)_i$ and $(Me–Zr)_0 \leftrightarrow (Me–Zr)_i$ exchange cross peaks, while, through the dissociation of the neutral borane (*d–r* process), the $(Me–B)_0 \leftrightarrow (Me–Zr)_i$ and $(Me–Zr)_0 \leftrightarrow (Me–B)_i$ cross peaks should be observed (Fig. 4). The experimental findings (Fig. 3) point to an *ips* mechanism, although this process is significantly slower than that observed for the corresponding non *ansa* derivatives, described above. No evidence of *d–r* process was found up to 340 K.

On the other hand, as found for the non *ansa* derivatives, in the presence of an excess of BAr_3, at 283 K, 2D EXSY showed $(Me–B)_0 \leftrightarrow (Me–Zr)_i$ and $(Me–Zr)_0 \leftrightarrow (Me–B)_i$ cross peaks, indicating the occurrence of a process that mimics the effects of a *d–r* exchange. Since the rate of a true dissociative process, like *d–r*, should not depend on the presence of BAr_3, this supports the idea that, in spite of its bulkiness, BAr_3 is able to attack the inward position of the *meso*-$[C_2H_4(4,7\text{-}Me_2Ind)_2ZrMe_{inw}]^+[MeBAr_3]^-$ complex and, through a bimolecular mechanism, interconvert the isomers.

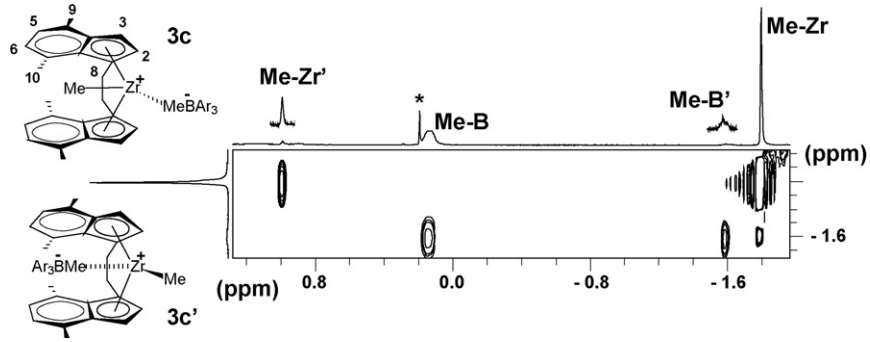

Fig. 3. Region of a ^{1}H EXSY experiment on a mixture of **3c** and **3c′** (320 K, toluene-d_8). The signals of **3c′** are magnified 12× in the insets above the 1D trace. The asterisk marks an impurity. Figure reproduced from ref. [30], with permission of the copyright holders.

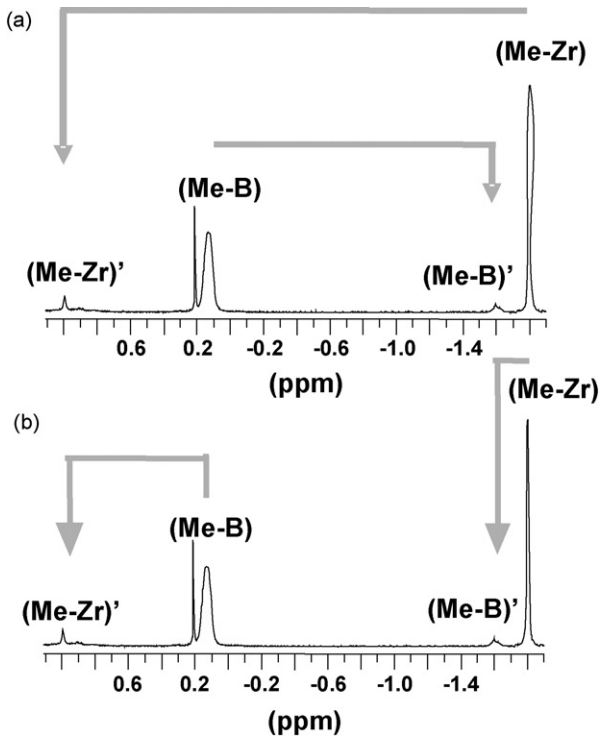

Fig. 4. A picture of the expected exchange patterns between the methyl resonances of **3c** and **3c**′, according to (a) *ips* or (b) *d–r* mechanisms. Figure reproduced from ref. [30], with permission of the copyright holders.

2.2. The interaction of $B(C_6F_5)_3$ with N-heterocycles

The relatively high coordinating ability of the $[MeBAr_3]^-$ anion, compared for instance to $[BAr_4]^-$ [10,13] or to the anions formed by the more encumbered tris(2,2′,2″-perfluorobiphenyl)borane, [28a] makes BAr_3 performances as co-catalyst less efficient than desired. The search for better co-catalysts explored the way of converting the Lewis acidity of BAr_3 into Brønsted acidity, enabling metallocene activation through protonolysis of the M–R bond with formation of a less coordinating anion [10].

The reaction of BAr_3 with aromatic five membered N-heterocycles afforded adducts with a high acidic sp^3 carbons (Chart 2) [31–33]. Archetypal pyrrole [31,33], and indole [31] derivatives (**5a** and **5b**) treated with NEt_3 gave instantaneously and quantitatively the corresponding borate anions [31], which are encumbered and poorly coordinating enough to be effective in the polymerization process. Indeed several adducts of this type proved to be active co-catalyst for metallocene-mediated ethylene polymerization with comparable or improved catalytic performances with respect to MAO or BAr_3 [34–36].

Likely, a significant contribution to the driving force for such easy deprotonation comes from the recovery of the aromatization of the heterocyclic ring. Interestingly, no acidic proton is present in the adduct obtained by the reaction of BAr_3 with indoline (**5f** in Chart 2) [31] neither such ability to protonate NEt_3 was observed for the adduct with 7-azaindole **5g**, where the interaction occurs exclusively on the pyridinic nitrogen [37].

The CH_2 hydrogen atoms of adducts **5a**–**5e** are diastereotopic and in their low temperature ^1H spectra they (but those of **5a**, see below) appear as an AB multiplet, that, on increasing the temperature, broadened and eventually coalesced into a singlet [31,32]. These compounds, due to the conformation of the perfluorinated rings, are examples of stereolabile conformational enantiomers.

The energy barriers for the rotation about B–C and/or B–N bonds are high enough to allow detection of these atropisomers through NMR spectroscopy. ^{19}F NMR confirmed this view, showing 15 distinct resonances. Similar conformational rigidity was observed also for adducts **5f** and **5g**.

Homonuclear (^1H and ^{19}F) and heteronuclear (^1H–^{19}F) scalar and dipolar correlation experiments allowed us to obtain the solution structure and a more detailed picture of the dynamic behaviour occurring in these compounds. In fact, other processes, besides the simple rotation around the bond connecting the borane and the heterocyclic moiety, can interconvert the two enantiomers.

The connectivities observed in 2D ^{19}F experiments for the *ortho* fluorine resonances resulted particularly useful to probe the solution structure. In fact ^{19}F COSY spectra provided, besides the straightforward assignment of the resonances of each ring, a not-obvious piece of information, showing "through space" coupling [38] between *ortho* fluorine atoms belonging to different rings (Fig. 5a). Nuclear spin–spin coupling via non-bonded interactions requires not only a short distance but also an effective lone-pair orbital overlap between the involved nuclei [38]. These scalar correlations integrate the evidence coming from ^{19}F NOESY experiments, since NOE cross-peak intensity can be significantly decreased by modulations due to such J coupling (Fig. 5b).

Moreover some of the *ortho* fluorine atoms showed scalar and dipolar correlations with the protons of the heterocyclic fragment, thus establishing its conformation with respect to the borane moiety, as illustrated in Fig. 6 for adduct **5c**.

The solution structures resulted strictly comparable with those obtained through single crystal X-ray analysis [31,37], showing the same $^{19}F\cdots{}^{19}F$ and $^1H\cdots{}^{19}F$ short contacts and the arrangement of the three rings typical of this class of compounds: one almost coplanar with the bond connecting the borane and the heterocyclic moiety (the so called *in-plane* substituent [39]), and the other two in a two-bladed propeller-like conformation (Fig. 7).

The 1D ^{19}F spectra show that more than one dynamic process is active in these adducts, as the resonances of the three rings undergo different broadening, on increasing the temperature. None of these processes implies the free rotation around the bond connecting boron to the heterocyclic moiety, since this would exchange all the three rings at same time. ^{19}F EXSY experiments pointed to two basic low energy processes, as shown in Fig. 8 for **5c**.

The first process, that leads to enantiomerization, implies the mutual exchange of the two aryl rings encompassing the most encumbered part of the heterocyclic fragment (the *in-plane* ring being one of these). The rings experience concerted small librations around their B–C_{ipso} bond, while the third ring flips [40]

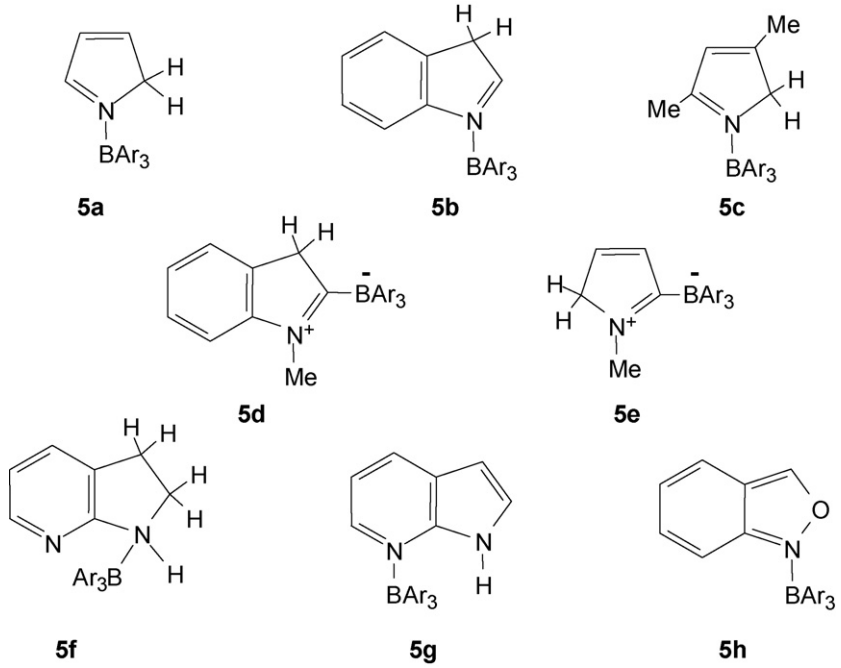

Chart 2.

and the heterocyclic fragment undergoes a small rotation around its bond with the boron atom. The second process exchanges the *in-plane* aryl group with the ring which was not involved in the previous exchange. Also in this case the heterocyclic moiety does not need to fully rotate around its bond with the boron atom.

The steric interactions between the heterocycle (and its substituents) and the borane moiety are likely the source of the rotation hindrance. The comparison of the room temperature ^{19}F spectra of three derivatives supports the view (Fig. 9): for the anthranyl derivative **5h** of Chart 2, where the oxygen in position 2 cannot establish any interaction, the exchange is so fast to give rise to a single signal, while for **5c** and **5b** the exchange is progressively slower. Moreover, in adduct **5a** (as in the one between indole and BCl_3) the methylenic protons appear as singlets at any temperature, due to the lack of any significant hindrance [31].

The rate constants of these processes can be obtained from the analysis of the volume of the exchange cross peaks (in particular in the *para* region, see Fig. 8) of suitable ^{19}F EXSY spectra [23,24] and from the band shape analysis of the ^{19}F and, when the case, ^{1}H 1D spectra [22]. The activation parameters derived accordingly for adducts **5b**, **5c** and **5g** indicate a much lower activation energy for **5c** compared to the indolic derivatives [31,37].

1D ^{1}H band shape alone is not recommended for the study of these dynamic processes since it is blind with respect to the real processes that are going on. Moreover, when the activation energies of the two processes are not very different (and in the range of a few degrees both become operative with comparable rates, as is the case of *N*-methyl derivatives), the derived rate constants and activation parameters are meaningless.

2.3. The interaction of $B(C_6F_5)_3$ with water

2.3.1. The Brønsted acid $[(C_6F_5)_3B(OH_2)]$ and its H-bonded adducts with water

The hydrolysis of BAr_3 to Ar_2BOH and eventually to $ArB(OH)_2$ and $B(OH)_3$ is very slow. However BAr_3 instantaneously reacts with water affording the adduct $[Ar_3B(OH_2)]$ (equilibrium 1).

$$BAr_3 + H_2O \leftrightarrows [Ar_3B(OH_2)] \quad (1)$$

In this way its strong Lewis acidity is converted into strong Brønsted acidity. Indeed $[Ar_3B(OH_2)]$, as the analogous adducts with alcohols, is able to protonate alkyl groups bound to metals, creating a vacancy that can be readily saturated by the coordination of the non-innocent borate anion $[Ar_3B(OR)]^-$ [41,42] or with the irreversible transfer of an aryl group to the metal [43].

The BAr_3/water system has been therefore thoroughly investigated by different groups. We completed the scenario framed by the X-ray structures of the two derivatives $[Ar_3B(OH_2)]$ [44] and $[Ar_3B(OH_2)]\cdot 2H_2O$ [45] and by the solution study in acetonitrile [46], in which the pK_a of $[Ar_3B(OH_2)]$ was found comparable with that of HCl in the same solvent.

Low and room temperature titrations with water of BAr_3 toluene solutions [47] proved the stepwise formation of the three mono-, di- and tri-aquo adducts $[Ar_3B(OH_2)]$ (**6a**), $[Ar_3B(OH_2)]\cdot H_2O$ (**6b**) and $[Ar_3B(OH_2)]\cdot 2H_2O$ (**6c**) (Chart 3), according to the equilibria 1, 2, and 3

$$[Ar_3B(OH_2)] + H_2O \leftrightarrows [Ar_3B(OH_2)]\cdot H_2O \quad (2)$$

$$[Ar_3B(OH_2)]\cdot H_2O + H_2O \leftrightarrows [Ar_3B(OH_2)]\cdot 2H_2O \quad (3)$$

The low temperature ^{19}F spectra, recorded while adding the first equivalent of water, showed two distinct signals for BAr_3

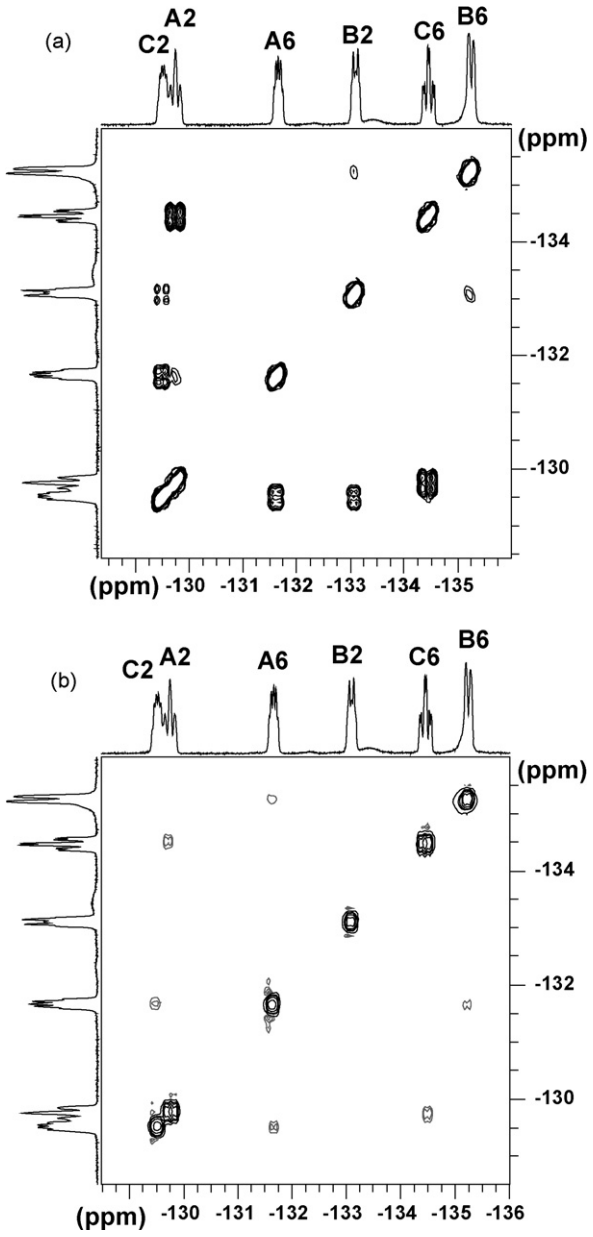

Fig. 5. (a) *Ortho* region of a ^{19}F COSY experiment on **5b** showing "through space" correlations between fluorine atoms of different aryl rings; (b) *ortho* region of a ^{19}F NOESY experiment on **5b**; all the cross peaks have opposite sign with respect to the diagonal peaks (233 K, toluene-d_8). Figure reproduced from ref. [31], with permission of the copyright holders.

and $[Ar_3B(OH_2)]$, indicating that the exchange of the B-bound water is slow on the NMR time scale. Instead, in the following titrations steps, a single set of signals was observed, the chemical shifts of which moved linearly upfield, particularly in the *para* region, as the amount of water increased (Fig. 10a). This evidence indicated that, also above 1 equiv of water, two species only were present in solution: the mono- and di-aquo adducts **6a** and **6b** below 2 equiv, and di- and tri-aquo adducts **6b** and **6c** above 2 equiv, respectively. Moreover the *para* signals were broad without fine structure between 1 and 2 equiv (Fig. 10b, left), while they were sharp and showed the typical pseudo triplet structure between 2 and 3 equiv (Fig. 10b, right).

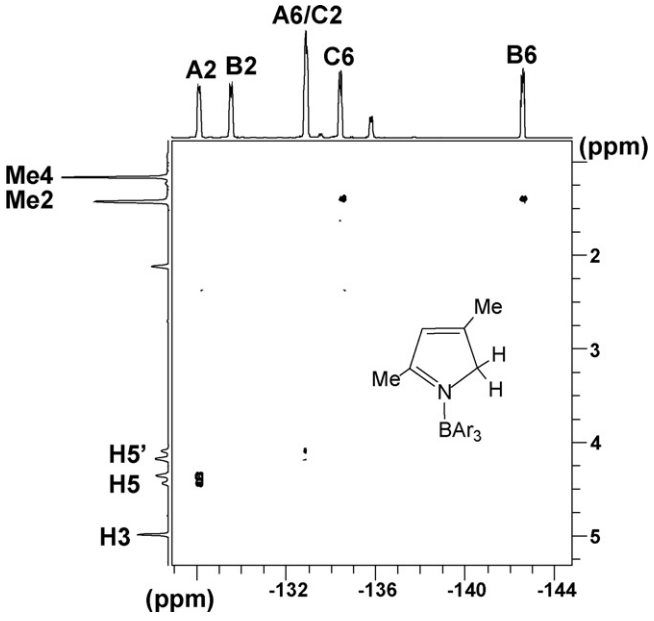

Fig. 6. [^{19}F–^{1}H] HOESY experiment on compound **5c** (185 K, toluene-d_8).

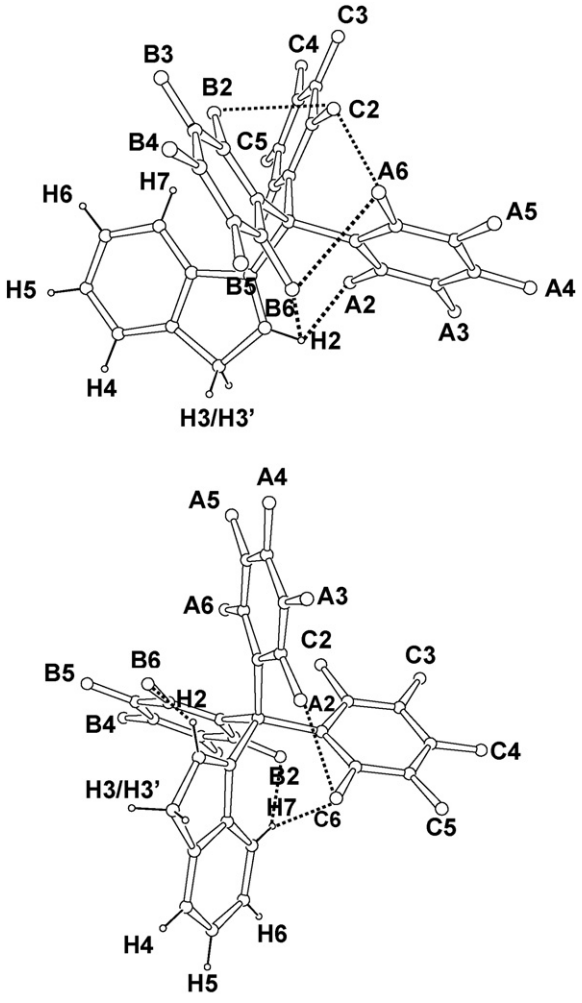

Fig. 7. Solution structure of compound **5b** as derived by ^{19}F–^{19}F and ^{1}H–^{19}F scalar and dipolar experiments. The dotted lines indicate the observed correlations. Figure reproduced from ref. [31], with permission of the copyright holders.

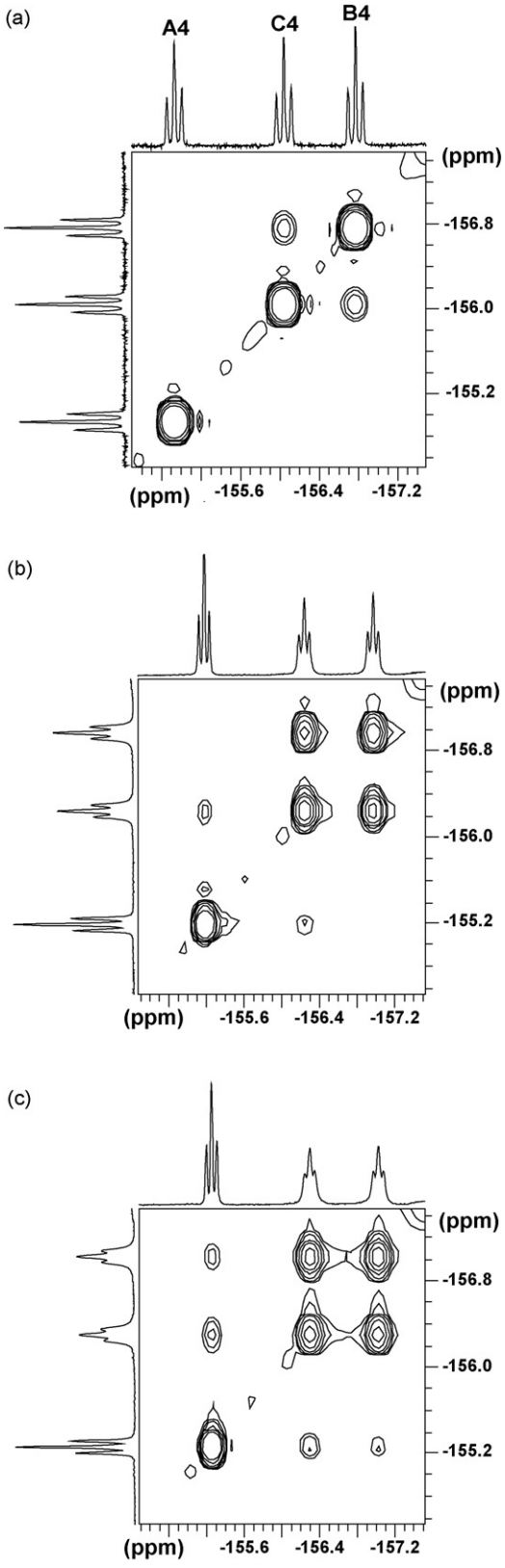

Fig. 8. *Para* regions of ^{19}F EXSY experiments on **5c** at (a) 253 K, (b) 278 K and (c) 284 K, showing the progressive onset of two exchange processes (toluene-d_8, $\tau_m = 50$ ms).

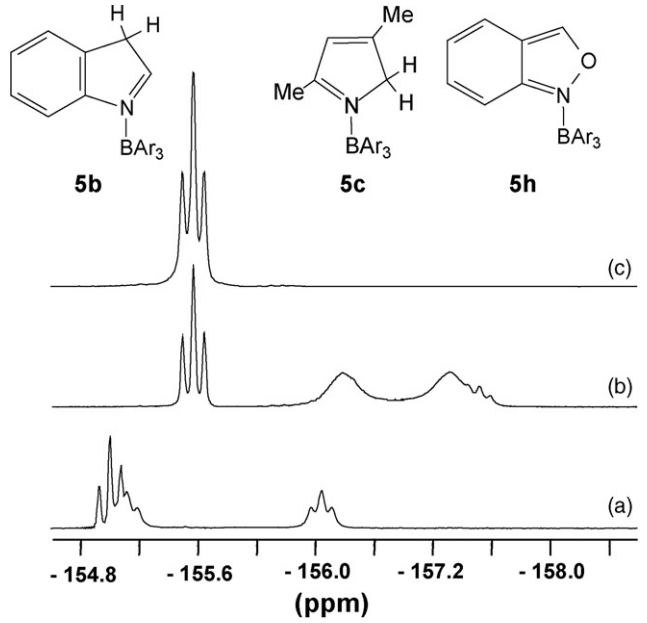

Fig. 9. *Para* region of ^{19}F spectra of compounds **5b** (a), **5c** (b) and **5h** (c) (300 K, toluene-d_8).

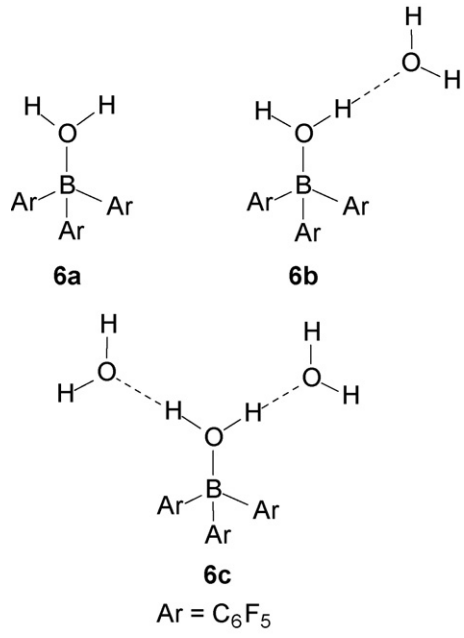

Chart 3.

Therefore even at 196 K fast dynamic processes exchange the H-bonded water molecules and the rate of these processes increase at higher water content. The ^{1}H spectra at 196 K confirmed the progressive quantitative reaction with water and the occurrence of dynamic processes.

Variable temperature experiments performed on samples with different concentrations at different water/BAr_3 ratios allowed us to have details on the intra- and intermolecular exchange processes active in this system. For many of them kinetic and activation parameters have been obtained through band shape analysis.

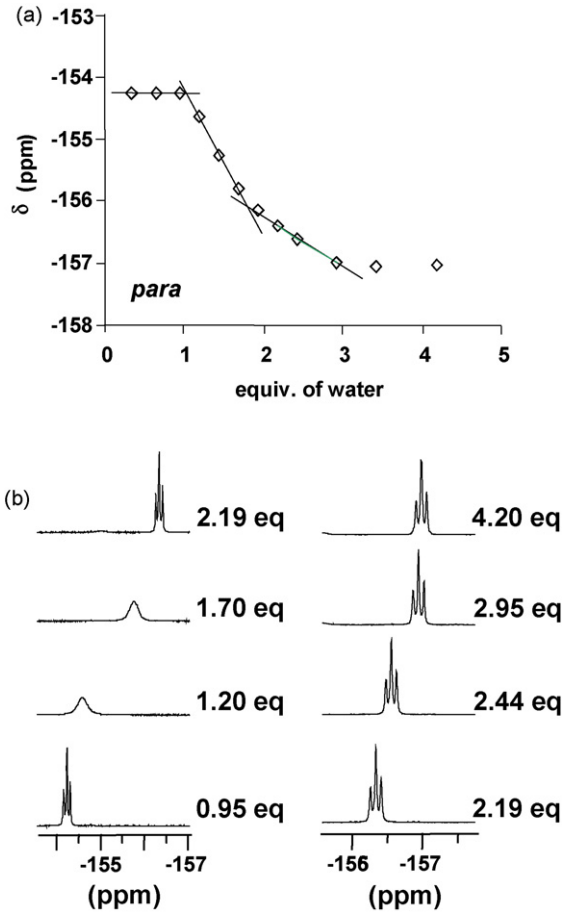

Fig. 10. (a) Variation of chemical shift of the *para* ^{19}F NMR resonances of the aqua species **6a**–**6c** during the titration of **1** with water, (b) selected spectra of the *para* region at different titration steps (196 K, toluene-d_8). Figure reproduced or redrawn from ref. [47], with permission of the copyright holders.

Below 1 equiv, the exchange of B-bound water, observable through ^{19}F, is the only dynamic process. Such exchange, slow at low temperature (*vide supra*), at room temperature is fast enough to give averaged signals. This is likely the reason for the scattered ^{19}F chemical shift values reported in the past for BAr_3, possibly due to a non-complete water removal from the solutions. Band shape analysis of the spectra of samples of different concentrations pointed to a dissociative process (the breaking of the bond between water and BAr_3 being the rate determining step). The activation parameters ($\Delta H^{\#} = 67$ (2) kJ/mol and $\Delta S^{\#} = 58$ (7) J/mol K) resulted in agreement with the previous work of Norton and co-workers [46].

Between 1 and 2 equiv, the H-bound water undergoes intermolecular exchange between **6a** and **6b**. A small temperature range was available for the kinetic studies of this process, since in ^{19}F spectra the 'near fast exchange' regime was already attained at 196 K and in the ^{1}H spectra above 210 K other exchange processes became evident. However mechanistic features were revealed by concentration dependence experiments in this temperature range: both unimolecular (dissociative) and bimolecular mechanisms contribute to the exchange of the H-bound water, the latter being more important in the range of concentrations investigated. Anyway, the rates of the dissociative pathway were more than four orders of magnitude higher than that of the dissociation of the B-bound water from **6a**, as expected for the lower strength of an hydrogen bond compared to a covalent bond.

The di-aquo derivative **6b** is involved in many dynamic processes, both inter- and intramolecular. In the presence of less than 2 equiv of water, the intermolecular exchange of the H-bonded water molecule occurs, as noted previously. When more that 2 equiv of water are present, analogously a H-bonded water molecule is exchanged with the tri-aquo adduct **6c**; in all conditions this last process is too fast on the NMR time scale to provide kinetic information. When the di-aquo adduct **6b** is the dominant species, other intramolecular processes become evident. First the external (H-bonded) water molecule moves so rapidly between the two hydrogen atoms of the internal (B-bonded) water that a single protonic signal is observed for the latter water. Above 210 K both the signals of the B-bound and H-bound water broadened, suggesting the occurrence of their mutual exchange. The rate constants were derived from the linewidth of the signal of H-bonded water in samples of different concentration and with composition very close to the exact stoichiometric ratio of 2 equiv. Their values (and that of the activation enthalpy) resulted close to those derived for the dissociative exchange of water between the mono-aquo adduct **6a** and BAr_3, supporting the idea that what occurs is not simple proton exchange but the interchange of the whole water molecules.

In the presence of the tri-aquo adduct **6c**, all the inter- and intramolecular processes became too fast to be studied through NMR.

It is interesting to remark that the presence of BAr_3 allows an amount of water much higher than its solubility to dissolve in toluene, even at very low temperature (for the typical concentrations used in our experiments just 0.2 equiv of water were above the saturation of toluene at 196 K).

2.3.2. *The Brønsted/Lewis base $[(C_6F_5)_3B(OH)]^-$ anion and its (labile) adducts*

The strong Brønsted acid $[Ar_3B(OH_2)]$ can easily be deprotonated by bases like NEt_3 or DMAN ('proton sponge', 1,8-bis(dimethylamino)naphthalene), affording the borate anion $[Ar_3BOH]^-$ [45,46] (**7** in Chart 4). In the presence of 1 equiv of BAr_3, the anion **7** behaves as a Lewis base and gives the dimeric borate $[Ar_3B(\mu\text{-}OH)BAr_3]^-$ (**8**) [45,48,49].

$$[Ar_3BOH]^- + BAr_3 \leftrightarrows [Ar_3B(\mu\text{-}OH)BAr_3]^- \quad (4)$$

This reaction is actually an equilibrium and, in the presence of other bases, **8** can act as a source of BAr_3 (in other words a single OH^- is not enough to neutralize the Lewis acidity of two BAr_3 molecules). For instance attempts at further deprotonating **8** with NEt_3, to obtain the corresponding dianion, resulted in reaction (5) between released BAr_3 and the amine [50].

$$2BAr_3 + 2NEt_3 \rightarrow [NHEt_3]^+[Ar_3BH]^- + Ar_3B^-(CH_2CH{=}N^+Et_2) \quad (5)$$

Even water was able to shift equilibrium 4 to the left, resulting in its insertion in the B–O–B bridge to give the

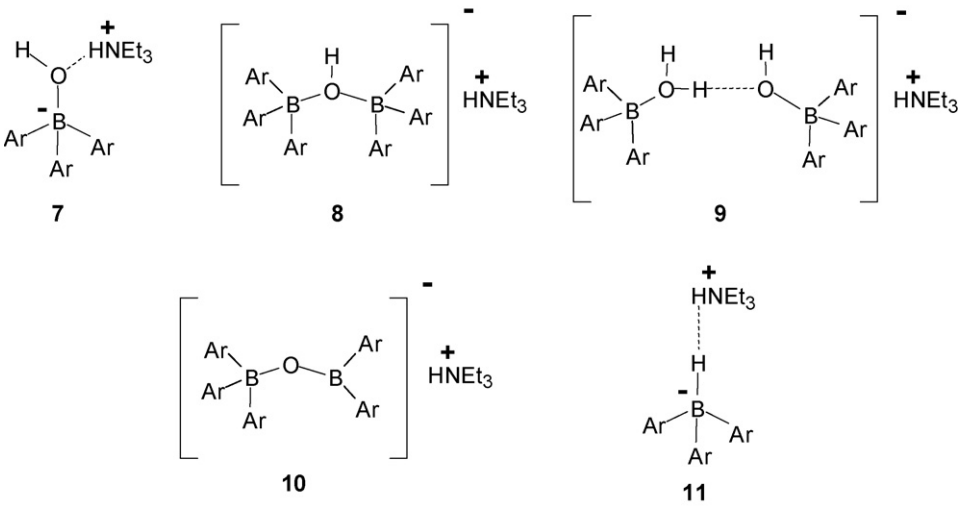

Chart 4.

$[Ar_3B(H)OH\cdots O(H)BAr_3]^-$ anion **9** [44,45,51].

$$[Ar_3B(\mu\text{-}OH)BAr_3]^- + H_2O \rightleftarrows [Ar_3B(H)OH\cdots O(H)BAr_3]^- \quad (6)$$

Reaction (6) can be explained by water coordination to BAr_3, followed by hydrogen bonding of **6a** to the borate anion **7**. Noteworthy, the reaction occurs even in the presence of adventitious water, so that **8** in solution behaves as water scavenger, as BAr_3. Rational and high yield synthesis of **9** are possible, e.g. by treating $[Ar_3B(OH_2)]$ with 0.5 equiv of NEt_3 or by treating $[Ar_3BOH]^-$ with 1 equiv of $[Ar_3B(OH_2)]$ [48].

The anion **9** can be viewed as a homoconjugated pair (of the Brønsted acid–base pair **6a/7**), or as the adduct between the $H_3O_2^-$ anion [52] and two BAr_3 molecules. The solution behaviour of di-borates **8** and **9** shows interesting differences. The ^{19}F low temperature spectrum of **8** indicates conformational rigidity, showing 15 fluorine signals (C_2 symmetry) for the three non-equivalent aryl rings. As in the case of the adducts of BAr_3 with *N*-heterocycles, the relative conformation of the three rings was obtained by the "through space" scalar couplings (Fig. 11) and dipolar correlations observed in ^{19}F 2D correlation experiments. The ^{19}F–^1H correlations assigned the *ortho* fluorine atoms close to the hydroxylic proton. This signal is a triplet (J_{HF} = 17 Hz) below 196 K and on rising the temperature becomes a 13-line multiplet, with an apparent J_{HF} = 3 Hz. This indicates the onset of dynamic processes that make equivalent all the *ortho* fluorine atoms of the six aryl rings. ^1H NMR cannot provide details about the nature of these dynamic processes. The cross peaks observed in the *para* and *meta* regions of ^{19}F EXSY showed instead how this equalization begins. At temperature as low as 183 K, mutual librations of the two borane moieties around the B–O bonds interconvert rings B and C, while wider oscillations interchange rings A and B with slightly slower rates (see Fig. 11d for the assignments) [48], as calculated from the volume of the exchange cross peaks in the *para* and *meta* regions [24].

The ^{19}F spectra of **9** showed a single set of fluorine signals (Fig. 11), only slightly broadened at low temperature, indicating that the interposition of the water molecule makes the rotation of the two borane fragments less hindered. The proton exchange within the $H_3O_2^-$ anion could instead be frozen. The single ^1H resonance (δ 8.55) observed at 300 K splits, below 173 K, into two resonances (1:2 ratio). The chemical shift of low field one (δ 17.9) is diagnostic of the occurrence of a strong hydrogen bond. The solution equivalence of the other two protons (δ 4.5), at variance with what observed in the solid state [48,52], points to a dynamic averaging due to the fast exchange of the hydrogen bonded proton between the two $[Ar_3BOH]^-$ moieties.

Free rotation of the aryl rings on the two boron atoms was observed also in the asymmetric borate $[Ar_3B(\mu\text{-}O)BAr_2]^-$ (**10** in Chart 4) [48], in which, the absence of proton/fluorine interactions and the presence of a trigonal boron fragment relieve rotation hindrance.

In our solution studies [48] we did not find evidence of close interactions between the borate anions **8** and **9** and their cations. Instead [^{19}F–^1H] HOESY showed that the anions containing a single boron center, namely $[Ar_3B(OH)]^-$ and $[Ar_3BH]^-$ (**11**), formed strong ion pairs with their $[NHEt_3]^+$ cations. In the case of $[Ar_3BH]^-$ this resulted in the formation of an unconventional hydrogen bond [53] between the negatively polarized hydride on the boron atom and positively polarized proton on the cation (Fig. 12). Such interaction was unambiguously detected only in a NOESY experiment performed under boron decoupling, being the hydride broad for the coupling with the quadrupolar boron.

As a final remark, water molecules are so effectively trapped by $[Ar_3B(H)OH\cdots O(H)BAr_3]^-$ that, when the countercation was $NHEt_3^+$, the corresponding N*H* resonance was not broadened by the exchange with water, as is usually the case for the NH protons. As a result, at room temperature the detailed fine structure due to the coupling to ^{14}N and to the six equivalent CH_2 protons of the ethyl groups (Fig. 13) could be observed, while at low temperature the increase of the ^{14}N relaxation rate caused the collapse of the multiplet.

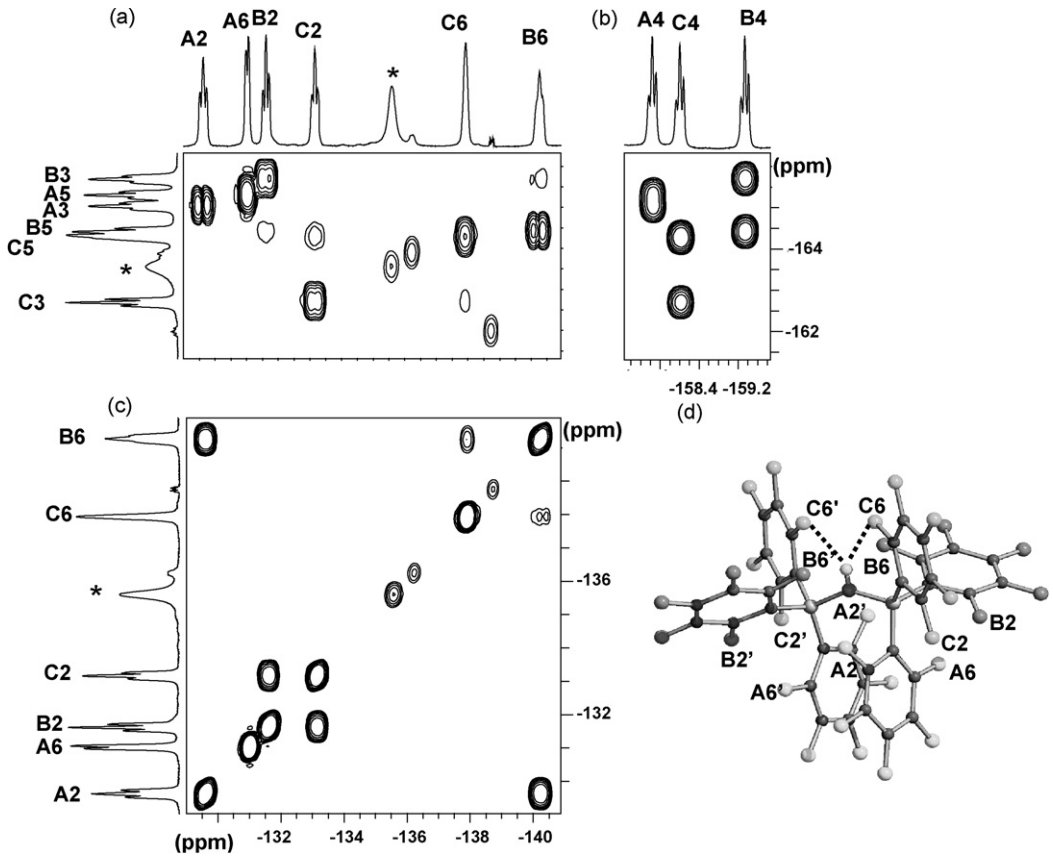

Fig. 11. (a–c) Selected regions of a ^{19}F COSY on compound **8** (173 K, CD_2Cl_2); panel (c) shows "through-space" scalar coupling in the *ortho* region. The resonances of compound **9**, present in the mixture, are marked with an asterisk; (d) the solution structure of **8** as inferred by NMR data. Figure reproduced from ref. [48], with permission of the copyright holders.

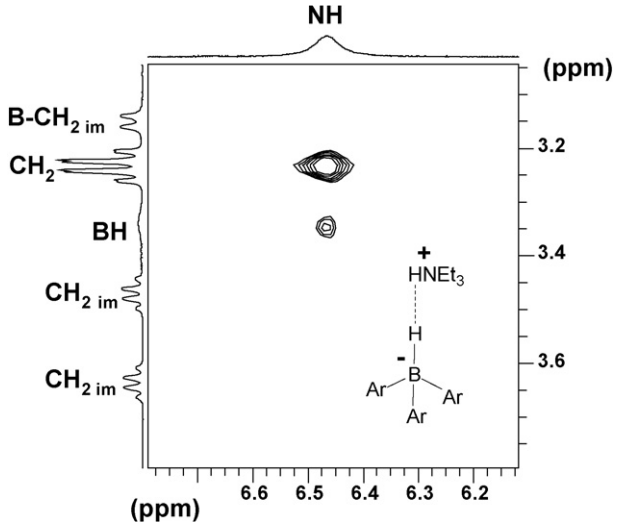

Fig. 12. $\{^{11}B\}^1H$ NOESY experiment on a mixture containing the ion pair $[NHEt_3]^+[(C_6F_5)_3BH]^-$ (**11**) and the zwitterionic imine $(C_6F_5)_3B^-(CH_2CH{=}N^+Et_2)$, showing the proton-hydride NH···HB interaction (298 K, CD_2Cl_2). The signals of the imine are marked with the pedix 'im'. Figure reproduced from ref. [48], with permission of the copyright holders.

3. The chameleonic nature of bis(pentafluorophenyl)borinic acid

Bis(pentafluorophenyl)borinic acid, Ar_2BOH (**2**, hereafter simply borinic acid) is an intriguing molecule. Due to its variety of active sites (Lewis and Brønsted acid, as well as Lewis base, and also hydrogen-bond donor and acceptor), in solution it is involved in manifold intra- or intermolecular interactions and association equilibria, so that it can dramatically modify its speciation in response to external stimuli, such as temperature, concentration, presence of even minimal amounts of bases.

It was first synthesized more than 40 years ago [8], but only in recent years has it been the object of intense investigations, both from academia [54] and industry [55]. The growing use of

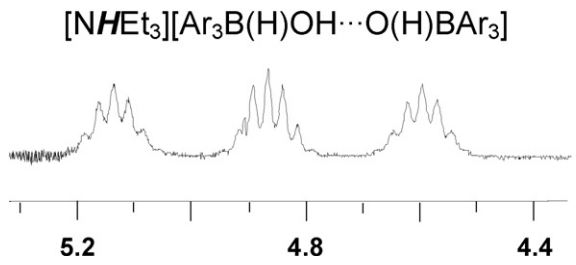

Fig. 13. NH region of the ^{1}H NMR spectrum of $[NHEt_3]^+$ **9** (298 K, CD_2Cl_2). Figure reproduced from ref. [48], with permission of the copyright holders.

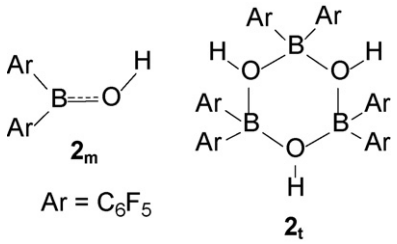

Chart 5.

this compound made a deeper investigation of the behaviour of **2** in solution more important.

At the beginning of our investigations on this molecule, we discovered that in the solid state **2** is a cyclic trimer, containing only tetra-coordinated boron atoms connected through oxygen-to-boron donor–acceptor bonds: *cyclo*-$(Ar_2BOH)_3$, $\mathbf{2}_t$ in Chart 5 [56,57]. This structure is unprecedented in organo-boron chemistry, where six-membered cycles always contain trigonal boron atoms, as for instance in boroxines, *cyclo*-$(RBO)_3$. Instead, this structure is much more similar to those of *cyclo*-$(R_2EO)_3$ siloxane and stannoxane derivatives.

A few Ar_2BX compounds (X = H, N_3), known to be dimers in the solid state, partly [58] or completely [59] dissociate when dissolved in aromatic solvents. This immediately raised the problem of the form in which **2** is present in solution: a trimer, a monomer, a different type of oligomer? And moreover: a single species or equilibrium mixtures? Our NMR investigations have brought to light a complex, and for many aspects surprising, behaviour, in which hydrogen-bonding interactions play a major role.

3.1. Toluene solution: a monomer with hindered rotation around the B–O bond

When **2** is dissolved in toluene, it very rapidly loses its trimeric nature: at room temperature all the NMR data [56,60] indicated the presence of a single species, and ^{11}B NMR, which provides information on the geometry around boron atoms [61], unambiguously assessed that this species is the monomer ($\mathbf{2}_m$). Indeed the chemical shift of the solution species (δ 42.2) falls in the range of tri-coordinated boron derivatives [62], while the solid phase exhibits a signal (δ 2.4) in the region typical for tetra-coordinated boron [63].

Such deoligomerization is clearly entropically driven. However, the trigonal boron atom in $\mathbf{2}_m$ can acquire some stabilization by π-donation from oxygen to the empty *p* orbital of boron. These pπ–pπ interactions are a common feature of trigonal boron compounds bearing substituents with non-bonding electron pairs [64]. The partial double bond character of the B–O interaction results in restricted rotation around the Ar_2B–OH bond (Scheme 2). The variable temperature ^{19}F spectra actually showed that at low temperature the two perfluoroaryl substituents of the boron atoms become not equivalent, while free rotation around the B–C_{ipso} bond is maintained, even at the lowest temperatures. Fig. 14 summarizes the most relevant NMR data concerning this process. A similar dynamical

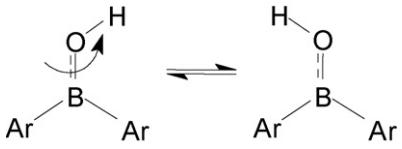

Scheme 2.

behaviour has been observed in several Ar_2BOR derivatives [65–67].

3.2. Self association in dichloromethane solution

On changing the solvent, the scenario drastically changes [68]. Dichloromethane solutions of **2** at room temperature always show two sets of signals, of different intensities, either in the ^{1}H or ^{19}F or ^{11}B spectra. One set of signals (the more intense) was immediately attributed to the monomeric form of borinic acid, for its strict resemblance with the data in toluene. The unambiguous attribution of the other set to the trimeric form was less straightforward and required some additional NMR experiments. Indeed ^{11}B (δ 8.4) told only that the unknown species contains tetra-coordinated boron. The values of the longitudinal relaxation times, much shorter than those of $\mathbf{2}_m$ [69], indicated a molecule bigger than the monomer. Its oligomeric nature was indicated by the increase of its relative amount on increasing the concentration and on decreasing the temperature, as it is typical of association equilibria. Finally, the trimeric nature of the oligomer was ascertained by measuring the slope of a suitable plot of the intensity ratios at different overall concentrations [68].

Therefore, in dichloromethane, a self-association equilibrium (7) is present, so that monomeric and trimeric forms of **2** coexist, in different relative amounts in different conditions. According to its lower dipole moment (computed values 0.75 Debye vs. 2.48 Debye for $\mathbf{2}_t$ and $\mathbf{2}_m$, respectively [68]), the equilibrium concentration of the trimer increases with decreasing solvent polarity, in the series CD_2Cl_2, $CDCl_3$ and CCl_4 [70] (Fig. 15).

$$3Ar_2BOH \leftrightarrows \textit{cyclo}\text{-}(Ar_2BOH)_3 \quad (7)$$

Variable temperature studies were performed to characterize this unusual association equilibrium. The spectra at the lowest temperatures revealed a completely unexpected process.

3.3. Spontaneous partial dehydration at low temperature

Whenever CD_2Cl_2 solutions of **2** are cooled below 220 K, small amounts of two new species are generated (see Fig. 16a), which disappear when the temperature is raised again. One of them was readily identified as the Ar_2BOBAr_2 anhydride (**12** in Chart 6) [60,71], formed according to equilibrium 8 [68].

$$2Ar_2BOH \leftrightarrows Ar_2BOBAr_2 + H_2O \quad (8)$$

The identification of the second species was much more difficult. Its formulation as the adduct **13a** depicted in Chart 6 is based on the relevant NMR evidence summarized in Fig. 16. The presence of bonded water was confirmed by the instanta-

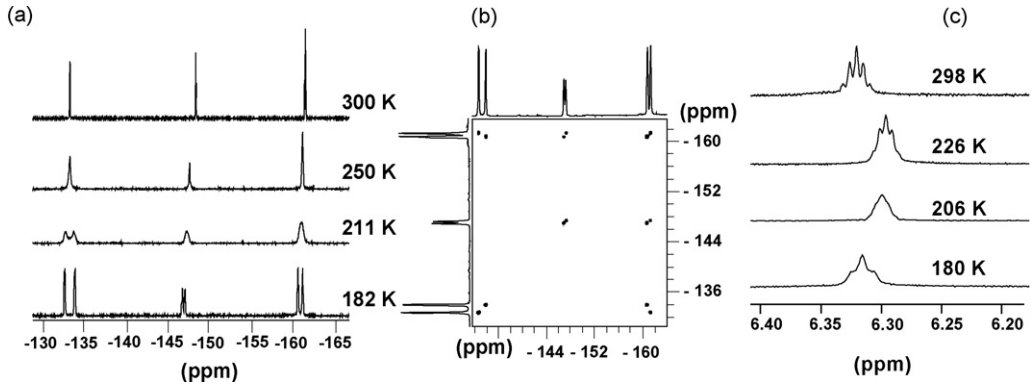

Fig. 14. (a) Variable temperature ^{19}F spectra of $\mathbf{2}_m$ showing the splitting of all the resonances. (b) ^{19}F COSY experiment showing separated scalar connectivities for each set of ^{19}F signals (188 K). Free rotation around the B–C_{ipso} bond averages the signals for the *ortho* and *meta* positions of each ring. (c) The ^{1}H resonance, a quintet at room temperature (averaged J_{H-F} = 1.6 Hz), at 180 K becomes a triplet (averaged J_{H-F} ca. 3 Hz), for the coupling with the two *ortho* fluorine atoms of one aryl ring only. Strong NOE with the same *ortho* fluorine atoms was also observed in a [^{19}F–^{1}H] HOESY at 180 K (not shown). Figures reproduced from ref. [56], with permission of the copyright holders.

neous and complete disappearance of the signals of **13a** upon addition of BAr_3 as water scavenger, and by the increase of its relative amount upon (small) addition of water. The hypothesis that water was simply hydrogen-bonded to $\mathbf{2}_t$ (giving the adduct **14a** of Chart 6) was ruled out by the ^{19}F EXSY experiment of Fig. 16c, which revealed that **13a** exchanges with $\mathbf{2}_m$, and not with $\mathbf{2}_t$.

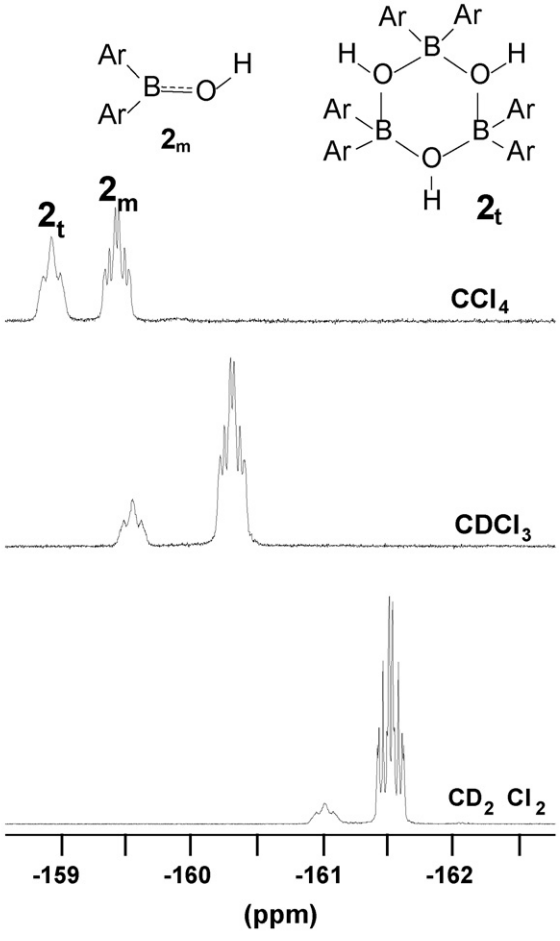

Fig. 15. *Meta* regions of ^{19}F NMR spectra of **2** in different solvents (0.1 M, 283 K).

The adduct **13a** is therefore constituted by an octa-atomic cycle, in which a proton is hydrogen bonded to the two identical ends of an open trimeric oligomer. An analogous of **13a** (namely **13c** in Chart 6) is formed in fair yield when borinic acid is treated with MeOH at 183 K [72].

Two remarkable features of **13a** must be stressed. First, the observed exchange of **13a** with $\mathbf{2}_m$ implies that, in spite of the strength of the hydrogen bond (δ 18.6 for the shared proton), the cycle is extremely labile, so that it is continuously destroyed and rebuilt, even at very low temperatures (rate constants of the order of 1 s^{-1} at 180 K).

Second, in spite of the lability of the system, the stabilization of the molecule of water in **13a** (where water is simultaneously covalently bound to a boron atom and hydrogen bonded to an oxygen atom) is so strong to promote water formation by dehydration of borinic acid itself to its anhydride. This process can occur only at very low temperatures, for entropic reasons, the overall equilibrium being represented by Eq. (9). Interestingly, this implies that low temperature solutions of borinic acid can be considered water scavenger more powerful than the anhydride itself!

$$5Ar_2BOH \leftrightarrows Ar_2BOBAr_2 + [(Ar_2BOH)_3{\cdot}H_2O] \quad (9)$$

As a result of the above described equilibria, low temperature dichloromethane solutions of pure borinic acid always contain four species: the monomer $\mathbf{2}_m$, the trimer $\mathbf{2}_t$, the anhydride **12** and the adduct **13a**.

3.4. The role of Lewis bases in the oligomerization equilibrium

The monomer–trimer equilibrium is affected by the presence of Lewis bases.

Since the beginning of our investigations, we realized that adventitious water was responsible for our initial erratic results [68], because its presence slightly increases the amount

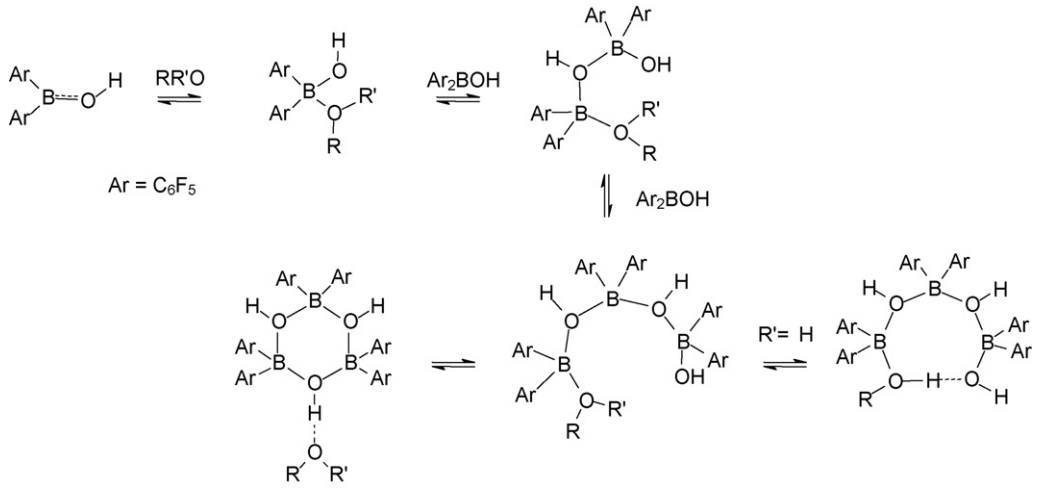

Scheme 3.

of trimeric species and notably increases the rate of the trimerization reaction. These effects varied with the relative amount of water, but were detectable even at very small water concentrations. Other Lewis bases caused similar (or even more dramatic) effects.

On working in the presence of BAr_3, as in situ water scavenger (standard dehydration of CD_2Cl_2 over molecular sieves being insufficient), we found that the true equilibrium concentration of the trimer at room temperature is rather small and, moreover, the attainment of the equilibrium is extremely slow. This prevented the acquisition of the thermodynamic parameters.

Why water and other bases are able to affect this sluggish equilibrium? The kinetic effect of the bases is due to their capability of opening alternative reaction paths. The association of borinic acid requires intermolecular oxygen-to-boron nucleophilic attack, but the intramolecular pπ–pπ O-to-B electron donation in $\mathbf{2}_m$ lowers both boron acidity and oxygen basicity. The coordination of bases to the boron atom of $\mathbf{2}_m$ (to give the adducts **15** of Chart 6) makes the non-bonding electrons of the OH group fully available for intermolecular interaction with another boron centre, so favouring the oligomerization process (see Scheme 3). PM3 calculations, performed for the interaction with water, supported this view [68].

The increase of trimer relative amount upon addition of small amounts of bases (clearly observable in the titrations monitored by ^{19}F NMR at 283 K, Fig. 17) is attributable to the stabilization of $\mathbf{2}_t$ by hydrogen bonding, giving adducts **14** of Chart 6 [73]. Indeed the H–bond of the base with $\mathbf{2}_t$ is favoured (with respect to that with $\mathbf{2}_m$), due to the higher acidity of the OH groups of $\mathbf{2}_t$. Notably, on increasing bases concentration, their effect on the monomer–trimer equilibrium is reversed, because equilibrium 10 is driven to the right and the trimeric species are destroyed (Fig. 17).

$$[(Ar_2BOH)_3\cdot\text{base}] + 2\text{base} \leftrightarrows 3Ar_2BOH\cdot\text{base} \quad (10)$$

Particularly impressive is what observed on using THF [74], which is a stronger Lewis base [75,76] and a better H-bond acceptor [77,78] than water. Upon addition of a stoichiometric amount of THF (0.33 equivalents), at 183 K, all borinic acid was instantaneously and quantitatively transformed into its trimeric form, stabilized by H-bond with THF (**14b** in Chart 6). On the contrary, the trimeric adducts with water (and MeOH) attained a high concentration at low temperatures only when the cooling of the solution was very slow, to allow the progressive shift of the equilibrium toward the trimeric form. Then the difference between THF and the other bases (water and MeOH) is mainly of kinetic nature. Why does this happen?

^{11}B monitoring of the titrations at 283 K (Fig. 18) made the picture still more puzzling, because it showed that for THF the preferential (although not exclusive) interaction with $\mathbf{2}_m$ occurred by H–bonding (**16b** in Chart 6) rather than by covalent bonding. The formation of the covalent adducts **15** was instead the dominant reaction with the other bases.

This evidence apparently contrasts with that expected for THF, taking into account its stronger Lewis basicity and its higher kinetic efficiency (which, according to Scheme 3, is based on the catalytic role of the covalent adduct). However: (i) THF is a stronger H-bond acceptor with respect to the other bases; (ii) its covalent adduct is slightly destabilized by steric crowding [79]; (iii) the covalent adducts with water (and MeOH) take benefit from intra- and intermolecular H-bond interactions [72]. As a result of this stabilization, the catalytic efficiency of these covalent adducts is reduced. On the contrary, the covalent adduct with THF (**15b**), although in minor concentration with respect to its isomer **16b**, is free to perform its role of initiator of the oligomerization process, just for the lack of other stabilizing interactions.

3.5. Ionization promoted by THF

When CD_2Cl_2 solutions containing the adduct between $\mathbf{2}_t$ and THF (**14b**) were treated further with THF, at 183 K, the unexpected formation of ionic species occurred, as revealed by conductimetric titrations. A detailed analysis of the NMR spectra [74] allowed us to recognize that the main products were two ionic species, namely the cation $[Ar_2B(OH_2)_2]^+$ and the anion $[Ar_6B_3O_3H_2]^-$, i.e. deprotonated $\mathbf{2}_t$ (**17** and **18**, respectively, in Chart 7).

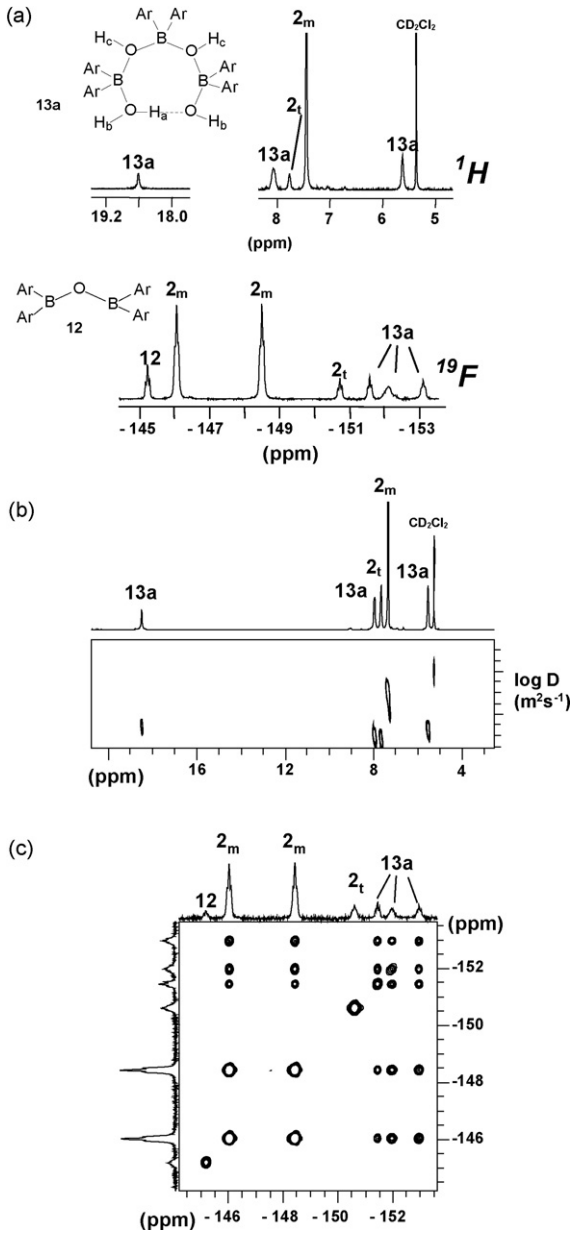

Fig. 16. (a) ^{1}H and ^{19}F (*para* region) spectra of CD_2Cl_2 solutions of **2** at 173 K. The three separate ^{19}F *para* signals indicate three non-equivalent Ar_2BOH units. The three ^{1}H signals (ratio 1:2:2) suggest the presence of a water molecule, involved in a strong hydrogen bond (δ 18.6). (b) ^{1}H DOSY experiment, in the same conditions, that shows the similarity of the diffusion coefficients of **13a** and $\mathbf{2}_t$. The overall pattern of the ^{1}H and ^{19}F resonances implies C_2 symmetry of the adduct. (c) *Para* region of ^{19}F EXSY experiment (184 K) showing that **13a** exchanges with $\mathbf{2}_m$, and not with $\mathbf{2}_t$. Figures reproduced from ref. [68], with permission of the copyright holders.

The four ^{19}F *para* resonances, in the ratio 1:1:2:2, observed for the anion $[Ar_6B_3O_3H_2]^-$ indicate a C_s symmetry, at variance with $\mathbf{2}_t$ or its adducts exocyclically H-bonded.

Many pieces of evidence support the (surprising) formulation of the cation [74]. Moreover, ^{1}H NOESY and [^{19}F–^{1}H] HOESY experiments suggested close proximity of THF to the cation. The downfield position of its protonic resonance (δ 13.4) shows that the interaction occurs by H-bonding.

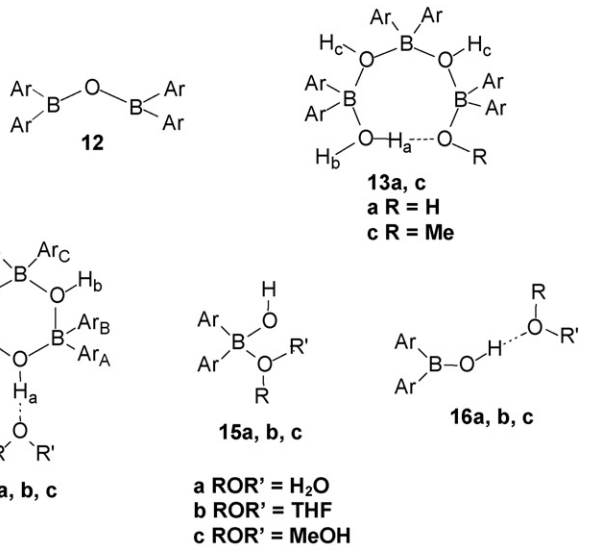

Chart 6.

Ions **17** and **18**, even at low temperature in CD_2Cl_2 constitute a loose ion pair. Indeed, no dipolar correlation was detected between the ^{1}H or ^{19}F signals of **17** and the ^{19}F resonances of **18**. This is probably ascribable to: (i) the high delocalization of the negative charge in the anion **18**; (ii) steric hindrance, which prevents a close approach of **17**–**18**; (iii) the relatively high dielectric constant of CH_2Cl_2 at low temperature [80], that favours ion separation. No ionization was observed by treating **2** either with H_2O or MeOH. This is due both to the higher Brønsted basicity of THF [81] and the low concentration of the key adducts of type **14** in the reaction conditions.

3.6. Intra- and intermolecular dynamic processes in $(C_6F_5)_2BOH$ and its derivatives

As already pointed out in the above survey, most of the species observed in solution are involved in intra- and intermolecular

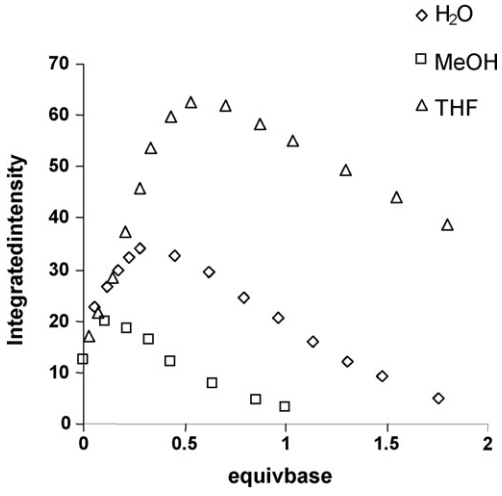

Fig. 17. Variation of the integrated intensities of trimeric species ($\mathbf{2}_t$ and its adducts) during the titration of **2** with bases (the overall intensity of trimeric and monomeric species set to 100).

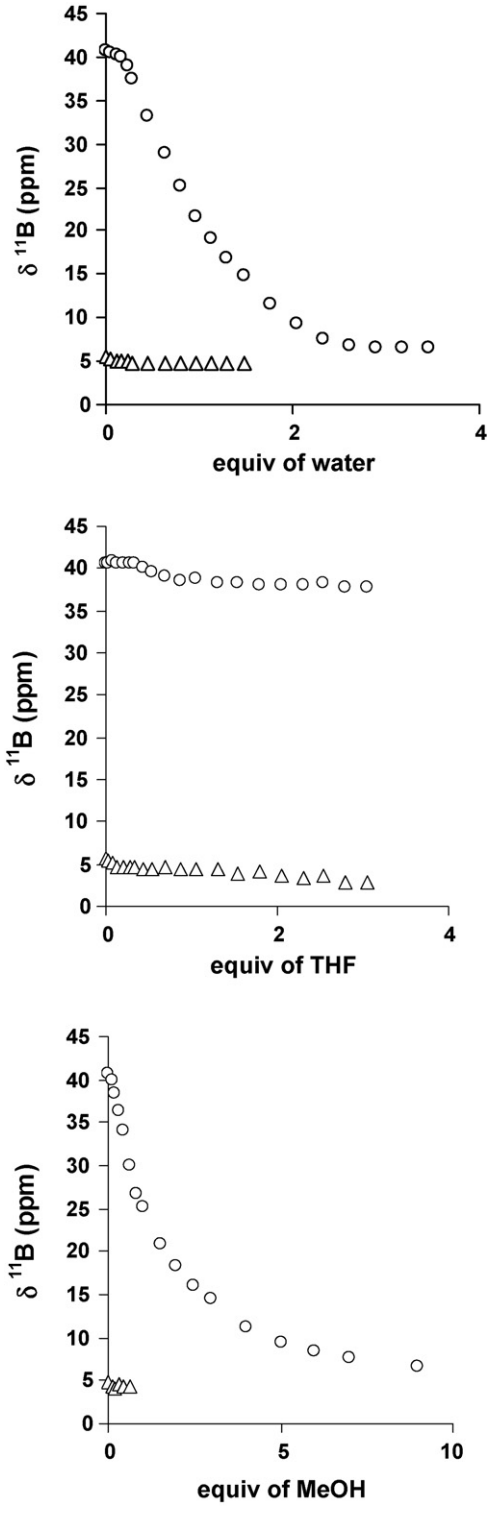

Fig. 18. Variation of the ^{11}B chemical shifts of the monomeric (●, averaged signals for $\mathbf{2}_m$ and its adducts) and of the trimeric species (▲, averaged signals for $\mathbf{2}_t$ and its adducts) in the presence of different amounts of bases (CD_2Cl_2, 283 K), showing the progressive shift of the signals of monomeric species from the region of tri- to that of tetra-coordinated boron in the titrations with water or MeOH. With THF, on the contrary, the signal of the monomeric species (dominant above 1 equiv, see Fig. 17) remained in the region of tri-coordinated boron. Upper panel reproduced from ref. [68] with permission of the copyright holders.

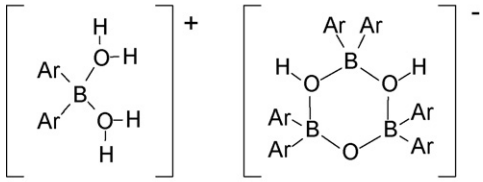

17 **18**

Chart 7.

exchange processes. In compounds containing tri-coordinated boron atoms, the partial double bond character of the B–O interaction makes the rotation around this bond hindered. Instead rotation of the perfluoroaryl rings around the B–C_{ipso} bond is free in the majority of these compounds, but in the adducts with bases of the cyclic trimer $\mathbf{2}_t$.

The behaviour of the adduct with THF (**14b**) was investigated in detail [74]. Its low temperature ^{19}F spectra (Fig. 19a) indicated a C_2 symmetry. A series of 2D correlation experiments at low temperature (Fig. 19 b–d) provided the structure shown in Figs. 19 and 20a. Close ^{19}F···^{19}F and ^{1}H···^{19}F contacts were detected in the 2D dipolar (and scalar) correlation experiments. Actually, PM3 computations showed that the insertion of a THF molecule in the pocket between the phenyl groups A and A′ of Fig. 20a distorts trimer geometry and leads to a more stiff conformation. Analogous close H···F contacts have been observed in all the other trimeric adducts of type **13** or **14**, and their OH signals usually appear as multiplets.

EXSY experiments performed at different titration steps revealed intermolecular exchange between **14b** and $\mathbf{2}_t$ (Fig. 20b). The values of the kinetic constants (obtained from the same EXSY experiments) increased roughly linearly with trimer concentration, with a non-zero intercept, showing that both dissociative and associative mechanisms contribute to this process [74].

On increasing the temperature, broadening and coalescence of all the ^{19}F resonances of **14b** occurs, leading to a single set of averaged signals indicative of an apparent D_{3h} symmetry. This implies the occurrence of three different dynamic processes: (i) the flopping of the cycle conformation, leading to equalization of the A/B rings of Fig. 20a; (ii) the rotation of the aromatic rings around their boron–carbon bonds, equalizing the *ortho* and *meta* positions within each ring; and then (iii) the exchange of THF among the three OH groups, leading to equalization of ring C with both A and B rings (Fig. 20c). Kinetic constants could be obtained from the cross-peak volumes for the *para* resonances only, and therefore the rate of process (ii) could not be determined. The invariance of the rate constants of process (i) in the titration course, agrees with the intramolecular nature of the cycle flopping process. On the contrary, the rate of the exchange of ring C with rings A and B was negligible at the beginning of the titration, then increased significantly, showing that process (iii) (THF migration) occurs by a bimolecular process (Fig. 20b–c).

The intramolecular dynamical behaviour of the adduct **14b** contrasts sharply with that of $\mathbf{2}_t$, which exhibits an apparent

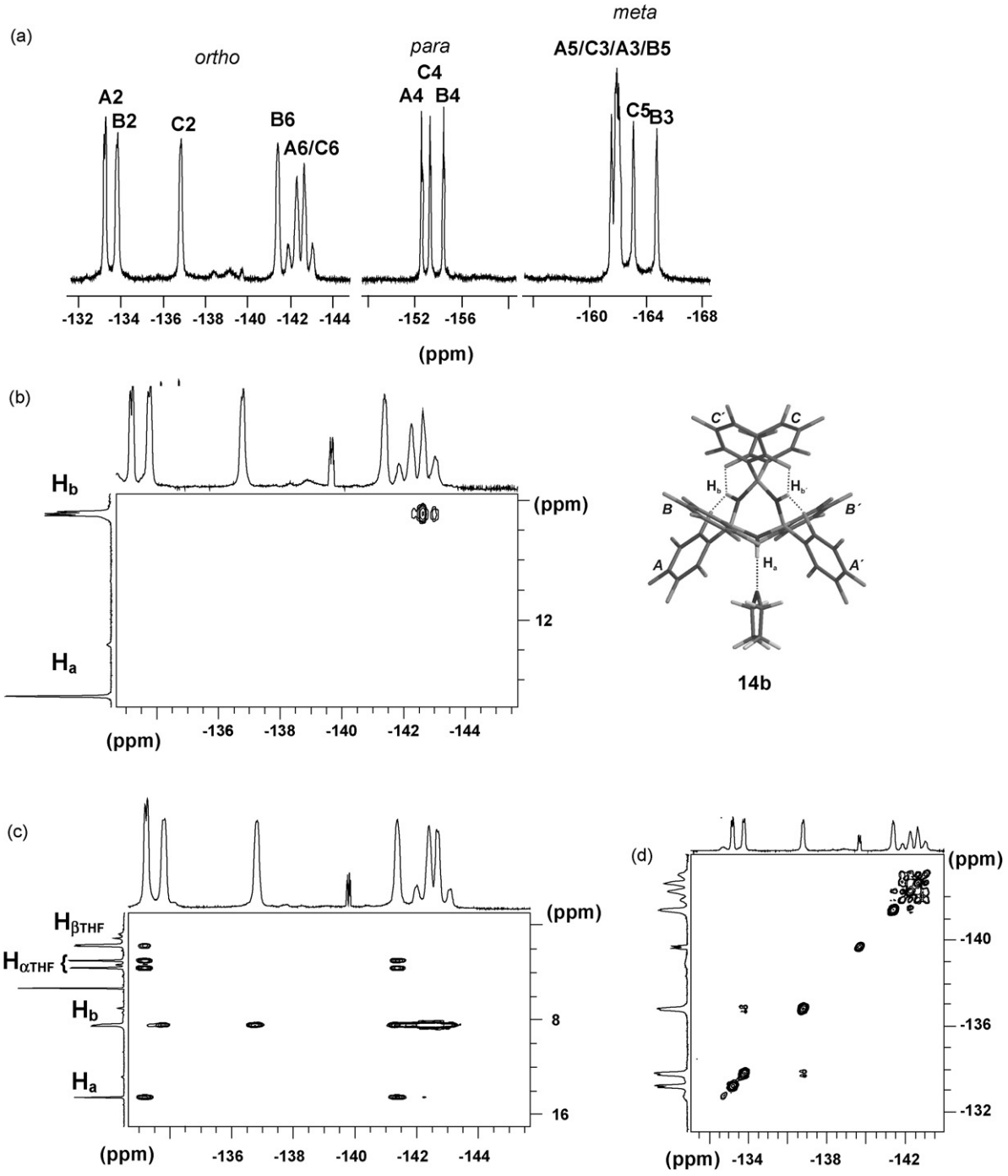

Fig. 19. (a) Relevant regions of the ^{19}F spectrum of **14b**. (b) [^{19}F–^{1}H] COSY, showing the correlation of H_b (δ 8.45) with two *ortho* fluorine atoms at highest field [82]; (c) [^{19}F–^{1}H] HOESY, showing the spatial proximity between the OH and THF protons and the *ortho* fluorine atoms; (d) section of a ^{19}F COSY showing the strong "through-space" coupling between *ortho* fluorine atoms at highest field, resulting in an AB system (J_{FF} = 115 Hz) (183 K, CD_2Cl_2). All the resonances are labelled according to Fig. 20a. Figure redrawn from ref. [74], with permission of the copyright holders.

D_{3h} symmetry also at the lowest temperatures, in spite of the C_2 symmetry observed in the solid state. PM3 computations accounted for this behaviour [74], showing the existence of a low energy path for a pseudo rotation of the trimeric ring which exchanges C_2 and C_s conformers, and, interchanging rings *C* with rings A and B, produces the observed apparent D_{3h} symmetry. This path is obviously forbidden for the adducts with bases.

The increased steric crowing among the different rings, resulting from the "insertion" of the THF molecule in **14b**, is likely responsible also for the freezing of the rotation around the B–C_{ipso} bonds, which on the contrary is free in $\mathbf{2}_t$. Similar hindrance is observed at very low temperature also in trimeric adducts **13** [68,72].

For adducts **13** fast intramolecular proton transfer along the hydrogen bond takes place. In **13a**, it was possible to (partly)

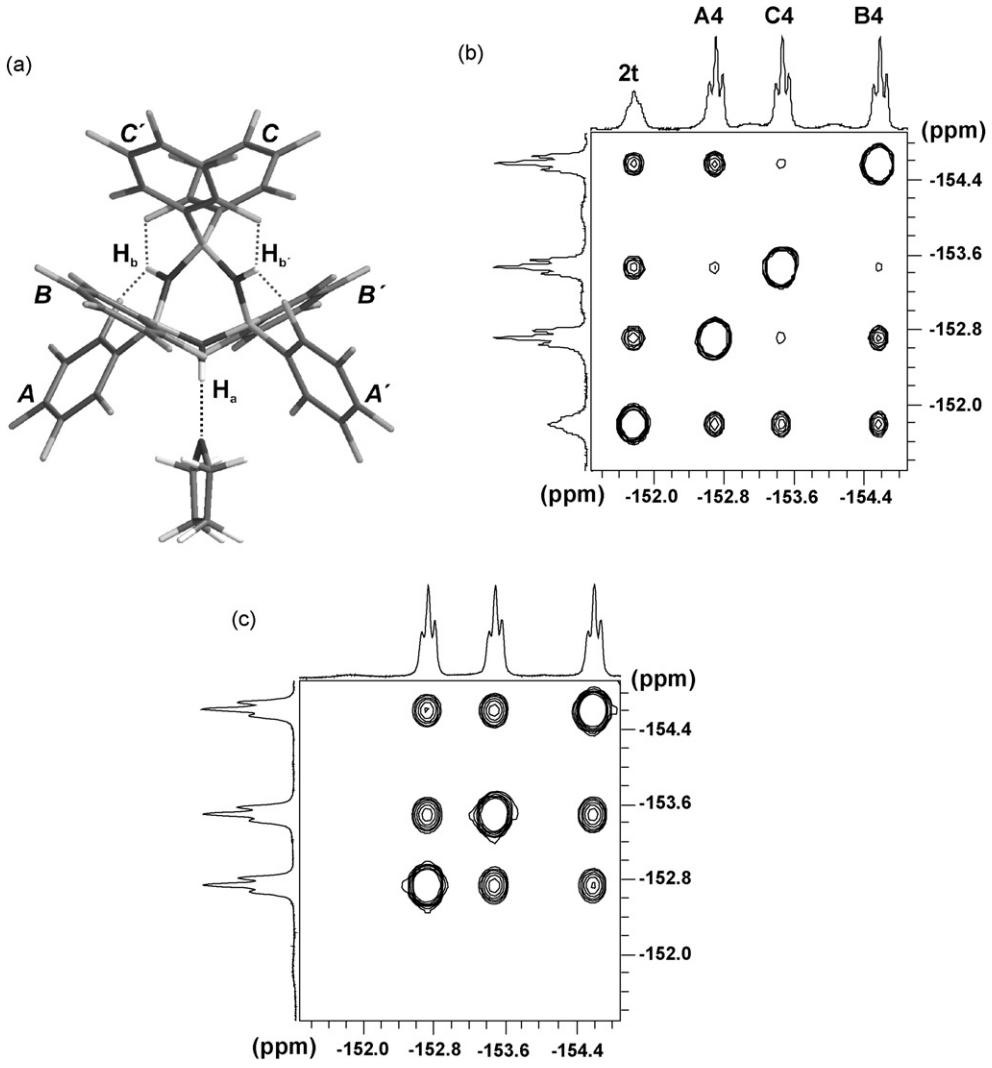

Fig. 20. (a) Stick model of adduct **14b**; para regions of ^{19}F EXSY experiments (183 K, CD_2Cl_2, $\tau_m = 0.15$ s) performed on a solution of **2** treated with THF showing: (b) after 0.18 equivalents the intermolecular exchange of **14b** with $\mathbf{2}_t$ and the intramolecular exchange between rings A and B in **14b**; (c) after 0.33 equivalents the increase of the rate of the exchange involving ring C.

freeze this process (in an overcooled sample), thus showing that the B(H)O···H···O(H)B hydrogen bond is not symmetrical and the C_{2v} symmetry, observed even at 183 K, is apparent [68]. Moreover as noted above (see Section 3.3) adduct **13a** is labile and borinic fragments exchange with $\mathbf{2}_m$. The two chain terminals generated by the proton transfer are identical, and the cross-peak volumes in ^{19}F EXSY experiments revealed that the aryl rings of the terminal Ar_2BOH units exchange with $\mathbf{2}_m$ at higher rate than those on the internal unit [68].

4. The diagnostic value of some NMR parameters

Chemical shifts, J couplings, and, in some instances, relaxation times are the fundamental NMR parameters for the characterization of unknown species in a chemical mixture.

For the systems described here, the use of relaxation time measurements was hampered by the individual existence of some species only in a restricted range of temperatures and most of all by the occurrence, even at low temperature, of intermolecular exchange processes, that averaged the relaxation rates. Only in the case of the (slow) equilibrium between the monomeric and trimeric borinic acid, are the relaxation data diagnostic.

The coupling data more relevant for the structure determination in these systems do not come from the normal "through bond" coupling, but instead, from the "through space" coupling. The congested geometry of many derivatives brings in spatial proximity both fluorine atoms belonging to different aryl rings (on the same or on adjacent boron atoms), and fluorine/hydrogen atoms. In this latter case, sometimes the ^{1}H signals change their multiplicitiy on varying the temperature as a result of dynamic processes. "Through space" ^{1}H/^{19}F couplings generally involve the *ortho* fluorine atoms and this interaction is, sometimes, apparent also in the high-field shift of the fluorine resonances [82].

Some more detailed comments will be devoted to the information provided by the chemical shifts.

4.1. The chemical shift of the H-bonded protons

A feature typical of ^{1}H low temperature spectra of the solutions containing borinic acid and bases is the presence of several signals at very low field, indicative of strong hydrogen bonds.

The resonances at the lowest fields are those of the trimeric adducts **13**, in which the H-bond connects the two opposite ends of an open oligomer, giving an octa-atomic ring: $\delta = 18.6$ and 17.0 for **13a** and **13c**, respectively [72]. The highest δ value is observed for the more symmetrical interaction, as expected.

Within the series of trimeric adducts **14**, exhibiting an exocyclic $\mathbf{2_t}$-base interaction, the order of downfield shift of the H-bonded resonance nicely correlates with the H-bond basicity [77] of the bases (and then with the H-bond strength): $\delta = 14.4$, 13.6 and 12.8 for THF, methanol and H_2O, respectively. The higher δ values found for the corresponding adducts **13**, containing the "endocyclic" hydrogen bond, agree with the expected greater strength of their hydrogen bonds, due to the higher symmetry of the moieties sharing the proton.

4.2. The separation between the meta and para ^{19}F resonances

In perfluoroaryl boranes ^{19}F NMR can provide a reliable (and often more easily accessible than ^{11}B) probe of the coordination around boron atoms [11,83]. Indeed the separation between the *meta* and *para* ^{19}F signals ($\Delta\delta_{m,p}$), which is large for neutral tri-coordinated boron compounds, progressively decreases on going to neutral tetra-coordinated boron centres and to anionic borates, due to the upfield shift of the *para* resonance(s), resulting from the shielding caused by the increased electron density on the boron atom. A rough empirical correlation between this parameter and ^{11}B chemical shift has also been previously evidenced, for the sensitivity of both the parameters to the electron density on the boron atom [11]. The data reported in Table 1 and depicted in Fig. 21a and b show that similar correlations nicely hold also for the compounds described here.

Actually, the prototypical trigonal species BAr_3 has the highest *meta-para* fluorine separation ($\Delta\delta_{m,p}$ 20) together with the lowest field ^{11}B chemical shift. The decrease of the values of δ ^{11}B and of $\Delta\delta_{m,p}$ on passing from BAr_3 to monomeric borinic acid and methyl borinate [72] agrees with what was previously observed on passing from BAr_3 to pentafluorophenate esters $Ar_{3-n}B(OAr)_n$ ($n = 1$, 2) [66] and it is possibly related to the oxygen-to-boron π-donation.

Coordination of bases, either to BAr_3 or to Ar_2BOH, lowers $\Delta\delta_{m,p}$ (to values in the range 6–8 ppm, as previously reported for analogous species [11]), and shifts the ^{11}B resonances (when available [84]) at δ typical for tetra-coordinated boron.

The trimeric form of borinic acid, its adducts with bases (**14**) and also the trimeric oligomers **13**, all show $\Delta\delta_{m,p}$ of about 9 ppm. The only ^{11}B signal available is that of $\mathbf{2_t}$, which lies in the tetra-coordinated boron group, as above mentioned.

Formal and real anionic charge on the boron atom decreases $\Delta\delta_{m,p}$, but the extent of such reduction depends also on the number of boron atoms and of aryl rings that delocalize the electron density. Interestingly among mono-boron anions such as $[Ar_3BOH]^-$, $[Ar_3BH]^-$ [85,86] and $[MeBAr_3]^-$, the highest $\Delta\delta_{m,p}$ (4.8, 3.7 and 5.0, respectively) are found when they form close ion pairs [87]; instead the lowest $\Delta\delta_{m,p}$ (2.2) is found for $[MeBAr_3]^-$, when it is the loose counterion of the dimeric metallocene cations [17,28b]. This is in line with that observed by Horton and de With [88], who proposed that the value of $\Delta\delta_{m,p}$ can be used to prove the existence of ion pairing between organometallic cations and $[RBAr_3]^-$ anions, since the delocalization of the negative charge in tight ion pairs shifts downfield the ^{19}F *para* resonance: values of $\Delta\delta_{m,p}$ lower than 3 ppm were taken as indicative of absence of interaction.

Nevertheless, the dinuclear anions $[Ar_3B(\mu\text{-}OH)BAr_3]^-$ and $[Ar_3B(H)OH\cdots O(H)BAr_3]^-$, that were shown to form a loose ion pair [48], have values of $\Delta\delta_{m,p}$ greater than 3 ppm (δ 5.2 and 5.6, respectively) due to delocalization of the negative charge on two BAr_3 units.

Analogously, the anionic trimer **18** shows a *para–meta* separation smaller than the neutral precursor $\mathbf{2_t}$ but larger than mono and dinuclear borates: $\Delta\delta_{m,p}$ 6.2 ppm vs. 9.7 ppm for $\mathbf{2_t}$ (Fig. 21a).

Table 1
Differences in chemical shifts between the *meta* and *para* fluorine atoms ($\Delta\delta_{m,p}$) and ^{11}B chemical shifts of the compounds here described

Compound	$\Delta\delta_{m,p}$ ^{19}F[a] (ppm)	^{11}B NMR[b] (ppm)
1	20.1	60.0
2m	13.7	43.8
2t	9.7	8.4
3a	5.0	−13.7
3b	5.0	−13.9
3c	4.8	−13.6
4	2.2	
5b	7.7	−3.5
5c	7.5	−8.25
5d	6.7	
5e	6.1	
5f	7.0	−0.79
5g	7.9	−3.6
5h	7.6	
6a	8.8	4.16
6b	8.1	
6c	7.5	
7	4.8	−4.4
8	5.2	−0.63
9	5.6	
10	5.1	
	9.1	
$Ar_3B^-(CH_2CH{=}N^+Et_2)$	4.6	−14.0
11	3.7	−24.4
12	15.4	40.1[c]
13a	9.4	
13c	9.1	
14b	9.1	
14c	9.2	
$Ar_2B(OMe)$	12.1[d]	40.7[d]
17	6.6	
18	6.2	

[a] The averaged values were considered in the case of inequivalent aryl rings.
[b] Boron data, when available, were obtained at room temperature.
[c] From ref. [60].
[d] From ref. [72]. The ^{19}F data are comparable with those reported in ref. [67].

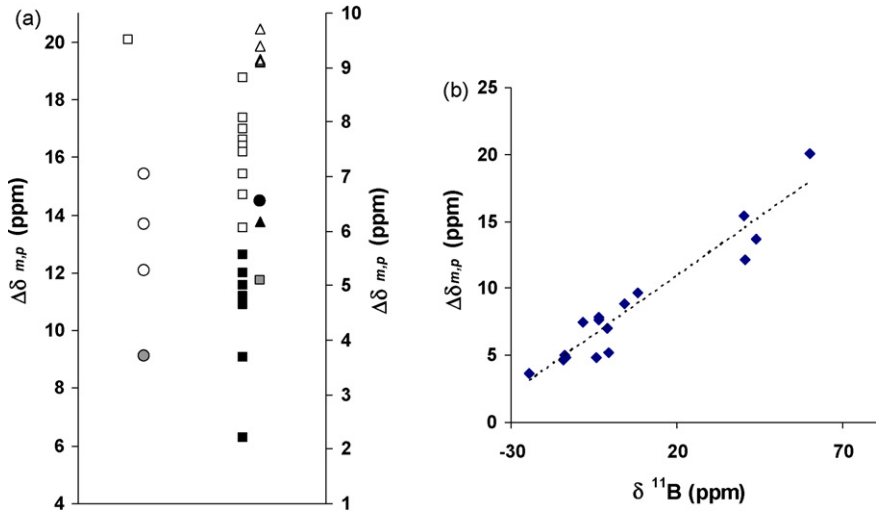

Fig. 21. (a) $\Delta\delta_{m,p}$ for the compounds described in this work. Left side: three-coordinated boron derivatives. Right side: tetra-coordinated boron derivatives. (□) $B(C_6F_5)_3$ derivatives, (◯) $(C_6F_5)_2BOH$ monomeric derivatives, (△) $(C_6F_5)_2BOH$ trimeric derivatives. Full symbols: ionic species; empty symbols: neutral species. Grey symbols are used for compound **10**. (b) Plot of ^{11}B chemical shift (δ ^{11}B) vs. the difference in chemical shift between ^{19}F *meta* and *para* resonances ($\Delta\delta_{m,p}$).

Finally, it is worthwhile to observe that the criterion holds also within a single species: the asymmetric dimeric anion $[Ar_3B(\mu\text{-}O)BAr_2]^-$, which contains both tri- and tetra-coordinated boron centers [48], shows different values of $\Delta\delta_{m,p}$ for the two centres (9.1 ppm and 5.1 ppm for the BAr_2 and BAr_3moiety, respectively).

5. Conclusions

The main conclusion that can be drawn from the studies here described is once again the tremendous effectiveness of NMR in disclosing a huge amount of sharp detail about the behaviour of fluoroaryl boranes in solution, in particular on their true speciation, intramolecular mobility and dynamic association equilibria, in several cases fully unexpected.

This information about the 'secret life' of these molecules is of primary importance for a better understanding of their basic chemical properties, but may also have relevance for understanding/designing applications in synthesis and catalysis. For instance, these studies have proved the relatively poor Lewis acidity of borinic acid compared with BAr_3. This may be of advantage in certain catalytic applications, where the easy reversibility of bonds activation is crucial. Moreover the importance of H–bond interactions, either in competing with the formation of Lewis acid–base adducts or in stabilizing some of them, has been established. Then the H–bond donor/acceptor capability of borinic acid may be synergistic in its interaction with substrates. Actually, hydrogen bonding is emerging as an effective tool in metal-free organocatalysis [89,90], and therefore both Lewis acid–base and H–bond interactions might be involved in the reactions catalysed by **2**.

Acknowledgements

The authors are indebted with Dr. L. Resconi (Basell Polyolefins) for having involved them into this field and for his stimulating comments and suggestions. Thanks are due also to Prof. A. Sironi and Dr. P. Mercandelli (CSSI Department of the Milan University) for their lucid contribution, supported by computational studies, to the understanding of the solution structures.

References

[1] E.R. Burkhardt, K. Matos, Chem. Rev. 106 (2006) 2617.
[2] D.G. Hall, Boronic Acids, Wiley-VCH, Weinheim, 2005.
[3] K. Smith, in: M. Schlosser (Ed.), Organometallics in Synthesis: A Manual, II ed., Wiley, Chichester, 2002.
[4] R.B. King, Ed. Boron, Chemistry at the millennium, J. Organomet. Chem. 581 (1999) 1.
[5] A. Suzuki, Pure Appl. Chem. 66 (1994) 213.
[6] H. Yamamoto (Ed.), Lewis Acids in Organic Synthesis, Wiley-VCH, Weinheim, 2000.
[7] (a) A.G. Massey, A.J. Park, J. Organomet. Chem. 2 (1964) 245;
(b) A.G. Massey, A.J. Park, J. Organomet. Chem. 5 (1966) 218.
[8] R.D. Chambers, T. Chivers, J. Chem. Soc. (1965) 3933.
[9] (a) S. Döring, G. Erker, R. Fröhlich, O. Meyer, K. Bergander, Organometallics 17 (1998) 2183;
(b) H. Jacobsen, H. Berke, S. Döring, G. Kehr, G. Erker, R. Fröhlich, O. Meyer, Organometallics 18 (1999) 1724.
[10] E.Y.-X. Chen, T.J. Marks, Chem. Rev. 100 (2000) 1391.
[11] W.E. Piers, Adv. Organomet. Chem. 52 (2005) 1.
[12] G. Erker, Dalton Trans. (2005) 1883.
[13] W.E. Piers, T. Chivers, Chem. Soc. Rev. 26 (1997) 345.
[14] X. Yang, C.L. Stern, T.J. Marks, J. Am. Chem. Soc. 113 (1991) 3623.
[15] X. Yang, C.L. Stern, T.J. Marks, J. Am. Chem. Soc. 116 (1994) 10015.
[16] H.H. Brintzinger, D. Fisher, R. Mülhaupt, B. Rieger, R.M. Waymouth, Angew. Chem. Int. Ed. Engl. 34 (1995) 1143.
[17] T. Beringhelli, G. D'Alfonso, D. Maggioni, P. Mercandelli, A. Sironi, Chem. Eur. J. 11 (2005) 650.
[18] D. Neuhaus, M.P. Williamson, The Nuclear Overhauser Effect in Structural and Conformational Analysis, Wiley-VCH, New York, 2000.
[19] (a) P.A. Deck, T.J. Marks, J. Am. Chem. Soc. 117 (1995) 6128;
(b) P.A. Deck, C.L. Beswick, T.J. Marks, J. Am. Chem. Soc. 120 (1998) 1772.
[20] A.R. Siedle, R.A. Newmark, J. Organomet. Chem. 497 (1995) 119.
[21] S. Beck, S. Lieber, F. Schaper, A. Geyer, H.H. Brintzinger, J. Am. Chem. Soc. 123 (2001) 1483.

[22] (a) J. Sandström, Dynamic NMR Spectroscopy, Academic Press, London, 1982;
(b) J.I. Kaplan, G. Fraenkel, NMR of Chemically Exchanging Systems, Academic Press, London, 1980.
[23] (a) R.R. Ernst, G. Bodenhausen, A. Wokaun, Principle of Nuclear Magnetic Resonance in One and Two dimensions, Oxford Science Publications, Oxford, 1987;
(b) J. Jeener, B.H. Meier, P. Bachmann, R.R. Ernst, J. Chem. Phys. 71 (1979) 4546.
[24] C.L. Perrin, D.J. Dwyer, Chem. Rev. 90 (1990) 935.
[25] S. Beck, M.H. Prosenc, H.H. Brintzinger, J. Mol. Catal. A: Chem. 128 (1998) 41.
[26] M. Bochmann, S.J. Lancaster, Angew. Chem. Int. Ed. Engl. 33 (1994) 1634.
[27] S. Beck, M.H. Prosenc, H.H. Brintzinger, R. Goretzki, N. Herfert, G. Fink, J. Mol. Catal. A: Chem. 111 (1996) 67.
[28] (a) Y.X. Chen, C.L. Stern, S. Yang, T.J. Marks, J. Am. Chem. Soc. 118 (1996) 12451;
(b) Y.X. Chen, T.J. Marks, Organometallics 16 (1997) 3649;
(c) Y.X. Chen, M.V. Metz, L. Li, C.L. Stern, T.J. Marks, J. Am. Chem. Soc. 120 (1998) 6287.
[29] (a) G. Guerra, L. Cavallo, G. Moscardi, M. Vacatello, P. Corradini, Macromolecules 29 (1996) 4834;
(b) L.A. Castoguay, A.K. Rappé, J. Am. Chem. Soc. 114 (1992) 5832.
[30] D. Maggioni, T. Beringhelli, G. D'Alfonso, L. Resconi, J. Organomet. Chem. 690 (2005) 640.
[31] S. Guidotti, I. Camurati, F. Focante, L. Angellini, G. Moscardi, R. Leardini, D. Nanni, P. Mercandelli, A. Sironi, T. Beringhelli, D. Maggioni, J. Org. Chem. 68 (2003) 5445.
[32] F. Focante, I. Camurati, D. Nanni, R. Leardini, L. Resconi, Organometallics 23 (2004) 5135.
[33] G. Kehr, R. Roesmann, R. Frölich, C. Holst, G. Erker, Eur. J. Inorg. Chem. (2001) 535.
[34] L. Resconi, S. Guidotti, Int. Pat. Appl. WO 01/62764 to Basell.
[35] A. Bonazza, I. Camurati, S. Guidotti, N. Mascellani, L. Resconi, Macromol. Chem. Phys. 205 (2004) 319.
[36] F. Focante, P. Mercandelli, A. Sironi, L. Resconi, Coord. Chem. Rev. 250 (2006) 170.
[37] F. Focante, I. Camurati, L. Resconi, S. Guidotti, T. Beringhelli, G. D'Alfonso, D. Donghi, D. Maggioni, P. Mercandelli, A. Sironi, Inorg. Chem. 45 (2006) 1683.
[38] (a) K. Köhler, W. Piers, Can. J. Chem. 76 (1998) 1249;
(b) F.B. Mallory, C.W. Mallory, K.E. Butler, M.B. Lewis, A.Q. Xia, E.D. Luzik Jr., L.E. Fredenburgh, M.M. Ramanjulu, Q.N. Van, M.M. Francl, D.A. Freed, C.C. Wray, C. Hann, M. Nerz-Strormez, P.J. Carroll, L.E. Chirlian, J. Am. Chem. Soc. 122 (2000) 4108;
(c) J.E. Peralta, V. Barone, R.H. Contreras, D.G. Zaccari, J.P. Snyder, J. Am. Chem. Soc. 123 (2001) 9162.
[39] D. Vagedes, G. Erker, G. Kehr, K. Bergander, O. Kataeva, R. Frölich, S. Grimme, C. Müch-Lichtenfeld, Dalton Trans. (2003) 1337.
[40] J. Brocas, M. Gielen, R. Willem, The Permutational Approach to Dynamic Stereochemistry, McGraw-Hill University Press, Cambridge, 1983.
[41] G.S. Hill, L. Manojlovic-Muir, K.W. Muir, R.J. Puddephat, Organometallics 16 (1997) 525.
[42] A.R. Siedle, R.A. Newmark, W.M. Lamanna, J.C. Huffman, Organometallics 12 (1993) 1491.
[43] H.A. Kalamarides, S. Iyer, J. Lipian, L.F. Rhodes, C. Day, Organometallics 19 (2000) 3983.
[44] L.H. Doerrer, M.L.H. Green, J. Chem. Soc., Dalton Trans. (1999) 4325.
[45] A.A. Danopoulos, J.R. Galsworthy, M.L.H. Green, S. Cafferkey, L.H. Doerrer, M.B. Hursthouse, Chem. Commun. (1998) 2529.
[46] C. Bergquist, B.M. Bridgewater, C.J. Harlan, J.R. Norton, R.A. Friesner, G. Parkin, J. Am. Chem. Soc. 122 (2000) 10581.
[47] T. Beringhelli, D. Maggioni, G. D'Alfonso, Organometallics 20 (2001) 4927.
[48] A. Di Saverio, F. Focante, I. Camurati, L. Resconi, T. Beringhelli, G. D'Alfonso, D. Donghi, D. Maggioni, P. Mercandelli, A. Sironi, Inorg. Chem. 44 (2005) 5030.
[49] (a) A.H. Cowley, C.L.B. Macdonald, J.S. Silverman, J.D. Gorden, A. Voigt, Chem. Commun. (2001) 175;
(b) M. Stender, A.D. Phillips, P.P. Power, Inorg. Chem. 40 (2001) 5314.
[50] N. Millot, C.C. Santini, B. Fenet, J.M. Basset, Eur. J. Inorg. Chem. (2002) 3328.
[51] M.J. Drewitt, M. Niedermann, M.C. Baird, Inorg. Chim. Acta 340 (2002) 207.
[52] (a) C. Bergquist, G. Parkin, J. Am. Chem. Soc. 121 (1999) 6322;
(b) C. Bergquist, T. Fillebeen, M.M. Morlok, G. Parkin, J. Am. Chem. Soc. 125 (2003) 6189.
[53] (a) J.C. Lee, A.L. Rheingold, B. Muller, P.S. Pregosin, R.H. Crabtree, J. Chem. Soc., Chem. Commun. (1994) 1021;
(b) A.J. Lough, S. Park, R. Ramachadran, R.H. Morris, J. Am. Chem. Soc. 116 (1994) 8356;
(c) R. Custelcean, J.E. Jackson, Chem. Rev. 101 (2001) 1963;
(d) N.V. Belkova, E.S. Shubina, L.M. Epstein, Acc. Chem. Res. 38 (2005) 624.
[54] (a) K. Ishihara, H. Kurihara, H. Yamamoto, Synlett (1997) 597;
(b) K. Ishihara, H. Kurihara, H. Yamamoto, J. Org. Chem. 62 (1997) 5664;
(c) K. Ishihara, H. Yamamoto, Eur. J. Org. Chem. (1999) 527.
[55] Recent patents dealing with synthesis or uses of 2 are;
(a) T. Sell, J. Schottek, N.S. Paczkowski, A. Winter, Patent WO 2006124231 (2006) to Novolen Technology;
(b) T. Neumann, S. Herrwerth, T. Reibold, H.-G. Krohm, Patent DE 102005004676 (2005) to Goldschmidt G.m.b.H.;
(c) R. Kratzer, Patent WO 04041871 2004 to Basell Polyolefins;
(d) R. Kratzer, Patent WO 04007570 2004 to Basell Polyolefins;
(e) R. Kratzer, V. Fraaije, Patent WO 04007569 2004 to Basell Polyolefins;
(f) K. Takei, K. Mizuta, K. Aoki, K. Takebe, Patent JP 2004265785 2004 to Nippon Shokubai;
(g) I. Ikeno, H. Mitsui, T. Iida, T. Moriguchi, Patent WO 0248156 2002 Patent to Nippon Shokubai Co;
(h) I. Ikeno, H. Mitsui, T. Iida, T. Moriguchi, Patent WO 0244185 2002 to Nippon Shokubai Co.;
(i) J. Schottek, C. Fritze, Patent DE 10009714 2001 to Targor;
(j) R. Kratzer, Patent DE 10059717 2001 to Basell Polyolefins;
(k) R. Kratzer, C. Fritze, J. Schottek, Patent DE 19962814 2001 to Targor;
(l) J.M. Frances, T. Deforth, Patent WO 0130903 2001 to Rhodia Chimie;
(m) J. Schottek, C. Fritze, H. Bohnen, P. Becker, Patent WO 0020466 2000 to Targor;
(n) H. Bohnen, U. Hahn, Patent DE 19843055 2000 to Aventis R&T GMBH;
(o) H. Bohnen, Patent DE 19733017 1999 to Hoechst A.-G.;
(p) H. Bohnen, H. Hahn, Patent WO 0017208 2000 to Aventis R&T GmbH.
[56] T. Beringhelli, G. D'Alfonso, D. Donghi, D. Maggioni, P. Mercandelli, A. Sironi, Organometallics 22 (2003) 1588.
[57] The existence of a solid state structure of 2 was previously mentioned in a footnote of R.A. Metcalfe, D.I. Kreller, J. Tian, H. Kim, N.J. Taylor, J.F. Corrigan, S. Collins, Organometallics 21 (2002) 1719.
[58] D.J. Parks, W.E. Piers, G.P.A. Yap, Organometallics 17 (1998) 5492.
[59] W. Fraenk, T.M. Klapötke, B. Krumm, P. Mayer, Chem. Commun. (2000) 667.
[60] J. Tian, S. Wang, Y. Feng, J. Li, S. Collins, J. Mol. Catal. A: Chem. 144 (1999) 137.
[61] R.G. Kidd, in: P. Laszlo (Ed.), NMR of Newly Accessible Nuclei, vol. 2, Academic Press, NY, 1983.
[62] Typical values for ^{11}B chemical shift in three-coordinated boron derivatives bearing pentafluorophenyl substituents are in the range 30 ÷ 80 ppm. See for instance ref 58, 59 and;
(a) G. Kehr, R. Fröhlich, B. Wibbeling, G. Erker, Chem. Eur. J. 6 (2000) 258;
(b) D. Vagedes, R. Fröhlich, G. Erker, Angew. Chem. Int. Ed. 38 (1999) 3362;
(c) B. Qian, D.L. Ward, M.R. Smith III, Organometallics 17 (1998) 3070;
(d) H. Nöth, H. Wahrenkamp, Chem. Ber. 99 (1966) 1049.

[63] The resonances for a neutral tetrahedral boron derivative containing pentafluorophenyl substituents are usually in the range $-20 \div +20$ ppm. See for instance the extensive compilation in ref. [11].
[64] N.N. Greenwood, A. Earnshaw, Chemistry of the Elements, 2nd ed., BH, 1998.
[65] P. Finocchiaro, D. Gust, K. Mislow, J. Am. Chem. Soc. 95 (1973) 7029.
[66] G.J.P. Britovsek, J. Ugolotti, A.J.P. White, Organometallics 24 (2005) 1685.
[67] S.P. Lewis, L.D. Henderson, B.D. Chandler, M. Parvez, W.E. Piers, S. Collins, J. Am. Chem. Soc. 127 (2005) 46.
[68] T. Beringhelli, G. D'Alfonso, D. Donghi, D. Maggioni, P. Mercandelli, A. Sironi, Organometallics 23 (2004) 5493.
[69] At 253 K, T_1 0.36, 0.44 and 0.57 s (vs. 1.95, 1.89 and 2.62 s in $\mathbf{1}_m$) for the ^{19}F *ortho*, *para* and *meta* resonances, respectively, and T_1 0.5 s (vs. 1.6 s in $\mathbf{1}_m$) for the ^1H resonances.
[70] $K = 3.9$, 10.2, 44.5, respectively, at 283 K, on passing from CH_2Cl_2 to $CHCl_3$ to CCl_4. The anomalous behaviour in toluene, where the trimeric form of borinic acid is below detection limits, in spite of the low polarity of the solvent, should be attributed to preferential solvation of the monomer, due to B–OH···arene interactions or to the higher availability of its aryl rings for interacting with the solvent aromatic rings.
[71] W.E. Piers, G.J. Irvine, C.V. Williams, Eur. J. Inorg. Chem. (2000) 2131.
[72] D. Donghi, D. Maggioni, T. Beringhelli, G. D'Alfonso, P. Mercandelli, A. Sironi, Eur. J. Inorg. Chem., doi:10.1002/ejic.200701210.
[73] The behaviour of 14a at very low temperatures is at present under investigation using freonic mixtures with the collaboration of Prof. H. H. Limbach (Freie Universität, Berlin).
[74] T. Beringhelli, G. D'Alfonso, D. Donghi, D. Maggioni, P. Mercandelli, A. Sironi, Organometallics 26 (2007) 2088.
[75] *Ab initio* studies on BF_3 affinities [76] have found the following Lewis basicity values for water, MeOH and THF 46, 65 and 82 kJ mol^{-1}, respectively (298 K).
[76] A. Rauk, I.R. Hunt, B.A. Keay, J. Org. Chem. 59 (1994) 6808.
[77] The parameter β_2, that measures the strength of a H-bond acceptor (or its H-bond basicity), is 0.51 in the case of THF, while water and MeOH have closer values (0.41 and 0.38, respectively) [78].
[78] M.H. Abraham, P.L. Grellier, D.V. Prior, J.J. Morris, P.J. Taylor, J. Chem. Soc., Perkin Trans. 2 (1990) 521.
[79] A PM3 computation showed that for THF the H-bonded adduct is more stable than the covalent complex (by about 12 kcal mol^{-1}), while for water the opposite holds [74].
[80] S. Gründemann, S. Ulrich, H.H. Limbach, N.S. Golubev, G.S. Denisov, L.M. Epstein, S. Sabo-Etienne, B. Chaudret, Inorg. Chem. 38 (1999) 2550.
[81] *Ab initio* studies on proton affinities have found the following Brönsted basicity values for water, MeOH and THF, 707, 766 and 832 kJ mol^{-1}, respectively (298 K) [76].
[82] S.J. Lancaster, A.J. Mountford, D.L. Hughes, M. Schormann, M. Bochmann, J. Organomet. Chem. 680 (2003) 193.
[83] J.M. Blackwell, W.E. Piers, M. Parvez, Org. Lett. 2 (2000) 695.
[84] For many derivatives of borinic acid it has been impossible the acquisition of the ^{11}B spectra, because either they were detected in mixtures or they exist only at low temperatures, where the ^{11}B resonances are usually exceedingly broadened by quadrupolar relaxation.
[85] A value of $\Delta\delta_{m,p} = 2.8$ ppm has been reported for a silyliminium salt of $[Ar_3BH]^-$ [86]. The slight difference with respect to our value might be due to a stronger ion pairing in the case of the $HNEt^{3+}$ salt, where a dihydrogen bond connecting cation and anion has been detected (see Section 2.3.2).
[86] J.M. Blackwell, E.R. Sonmore, T. Scoccitti, W.E. Piers, Org. Lett. 2 (2000) 3921.
[87] The zwitterionic species Ar_3B^- ($CH_2CH{=}N^+Et_2$) [48] shows a behaviour analogous to that of the anions here discussed ($\Delta\delta_{m,p}$ 4.6), in agreement with the negative charge on the boron moiety.
[88] A.D. Horton, J. de With, Organometallics 16 (1997) 5424.
[89] P.R. Schreiner, Chem. Soc. Rev. 32 (2003) 289.
[90] P.M. Pihko, Angew. Chem. Intern. Ed. 43 (2004) 2062.